Master of Science

EFFECTS OF SOLID/FLUID BOUNDARY DEFINITION ON ESTIMATING NANOSCALE PHENOMENA: A MOLECULAR DYNAMICS STUDY

Yechan Aaron Noh

The Graduate School

University of Ulsan

School of Mechanical Engineering

June 2018

EFFECTS OF SOLID/FLUID BOUNDARY DEFINITION ON ESTIMATING NANOSCALE PHENOMENA: A MOLECULAR DYNAMICS STUDY

Academic advisor: Professor BoHung Kim

A Thesis

Submitted to the Graduate School of the University of Ulsan

In partial Fulfillment of the Requirements for the Degree of Master of Science

By

Yechan Aaron Noh

The Graduate School

University of Ulsan

School of Mechanical Engineering

June 2018

EFFECTS OF SOLID/FLUID BOUNDARY DEFINITION ON ESTIMATING NANOSCALE PHENOMENA: A MOLECULAR DYNAMICS STUDY

This certifies that the thesis is approved.

Committee Chair Prof. Jichul Shin

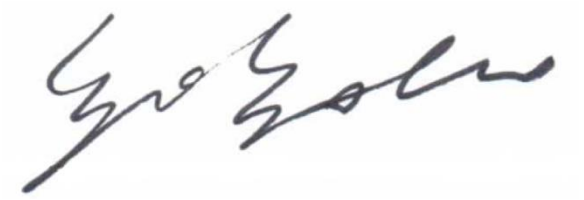

Committee Prof. KyoungSik Chang

Committee Member Prof. BoHung Kim

The Graduate School

University of Ulsan

School of Mechanical Engineering

June 2018

Acknowledgment

Firstly, I genuinely thank Professor BoHung Kim for his guidance in my academic career and life. He guided me to the promising academic subject and taught me world-class research skill to become an independent researcher. Also, I was able to study in a pleasant environment without financial worries. With his guidance for about four years, my perspective has been broadened, and I have come to the broader world. Without him, I would not have been able to imagine my accomplishment now.

Also, I would like to express sincere gratitude to Ph.D. Vo. He helped me a lot with valuable discussions on Molecular Simulation of the nano-fluidics system. If it were not for him, I would have had a tough time getting into the academic field. I also thank MNTF members for sharing many memories with me. Booseong always treated me kindly. I am fortunate to be able to work with Emily, who is always friendly and cares about the LAB members like a mother. Gyoung Hun and Rashedul also have many interactions with me during my Master. The memory with you will be forever in my entire life.

I really appreciate to all my friends in Ulsan, especially Hyo Jin Kim and Hyun Jin Park. The memory that we had together is a great pleasure during 5 years in Ulsan. Such memories made me able to concentrate more on my studies without any depressions. I would like to say that they are paragons of a good friend. Thank you for sharing all emotions with me all the times.

I also express my gratitude to my beloved family members. Without your dedicated support, I would not have been able to continue my studies. Thank my mother who always

supports and respects my dream. My fruits during undergraduate and graduate school have come from my mother's sweat. I am also grateful that my father has always guided me in a right and humane direction. Also, I appreciate the effort of my older sister, who know and understand me best in this world.

Lastly but the most important, I would like to express my heartfelt gratitude toward my wife, Minju. She believed in me and supported me all the time. Inter alia, I really appreciate her having been with me at the toughest time when I prepared daunting exams for studying abroad. Without her encouragement, I would not have been able to achieve this much. I express inestimable gratitude to her for respecting and following me by belief.

Abstract

Effects of Solid/Fluid Boundary Definition
on Estimating Nanoscale Phenomena:
A Molecular Dynamics Study

(June 2018)

Yechan Aaron Noh

In this work, we investigate the atomic-level wall/fluid boundary to properly analyze nanochannel heat transfer using molecular dynamics (MD) simulations. In the absence of an atomic-level boundary definition, the wall/fluid boundary has been differently defined within one atomic diameter. This amount of discrepancy of boundary definition can cause significant impacts on the computed observables in small scale. To clarify these impacts, we conducted heat transfer MD simulations of liquid argon confined between two silver walls. The fluid density, heat flux across the channel, and the fluid thermal conductivity were calculated with respect to the different definitions of wall/fluid boundary. Our results reveal that one atomic diameter boundary shift causes relatively large deviations between the computed and the preset values. In addition, these variations become more significant as the channel height decreases. It is shown that the uncertainty atomic-level boundary definition can create not only a quantitative but also qualitative discrepancy. We also specify wall/fluid boundary in atomic accuracy using microscopic heat flux equation. The location shows a good agreement with literature and zero-potential

location of wall molecule where is the wall boundary at absolute zero temperature. The findings in this work provide atomic-level insights into the wall/fluid boundary, as well as useful information on the design of nano-devices aimed at energy optimization.

Table of Contents

List of Tables

List of Figures

1. Introduction

The recent rapid development of nanotechnology has motivated the need for understanding of molecular-level physics to model various nano-devices such as energy storage [1], water purification [2, 3], Gas separation [4], Drug delivery [5], thermoelectric generators [6, 7], Nanopower generator [8] and biochip [9, 10]. In order to accurately model nanoscale physics, it is crucial to understand interfacial phenomena, as it plays a dominant role in small scale. However, the molecular level detail of interfacial phenomena is difficult to be accessed by experiment. Currently, nanoscale experiments are only possible to a limited extent and have limitations. For example, the current resolution of local temperature measurement is about 100nm scale, which is too rough to measure the local temperature in nanotubes currently investigated (~0.1nm). For the investigation of nanoscale physical phenomena including heat and mass transfer, Molecular Dynamics (MD) simulations have alternatively been used. The atomistic simulation provides all atomic trajectories by solving equations of motions of all atoms. The aggregation of the molecular movements, ensemble average, can be converted into the physical properties and it has shown good agreements with theoretical and experimental value [11-18]. Even though the MD simulation has limitations in quantitative predictions of interfacial phenomena because of its sensitivity to the interatomic parameter [19], the insights from MD simulation into the microscopic phenomena is valuable. Hence, MD simulation has been widely used to understand microscopic behavior including interfacial phenomena.

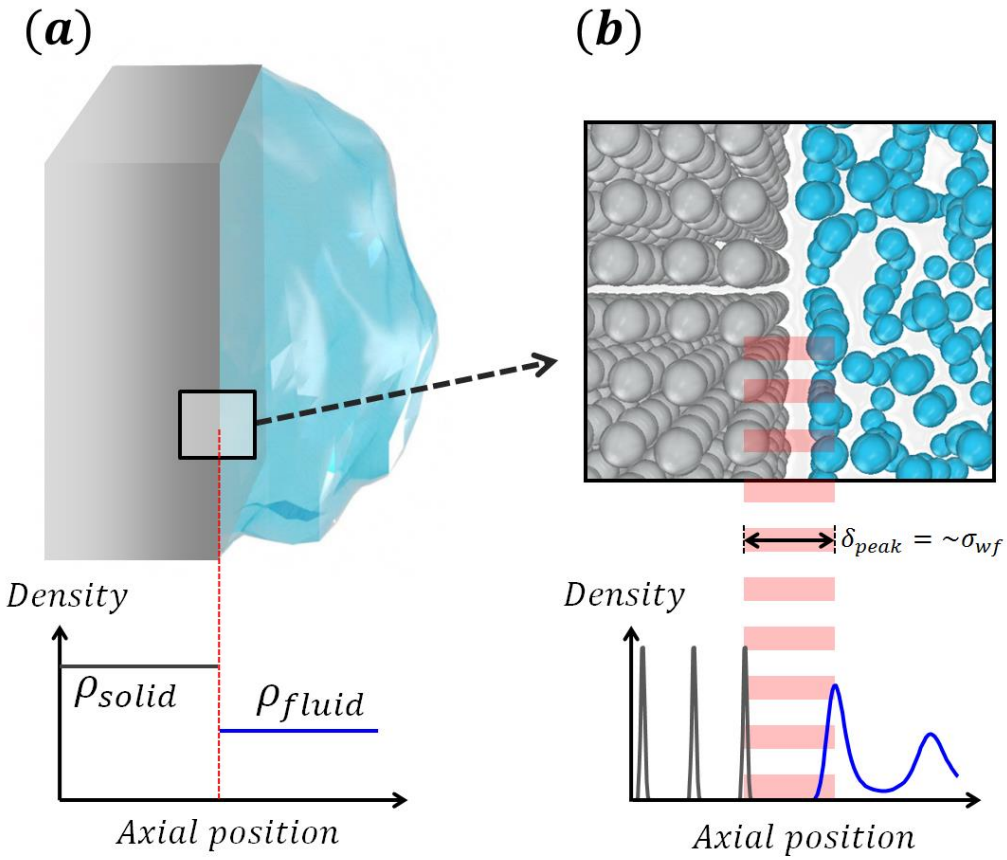

Figure 1 Graphical representation of wall/fluid boundary at two different scales

Since computer simulations allow access to the scale that is smaller than an atomic diameter, a new question has been raised about the precise definition of wall/fluid interfaces. At the molecular scale, the wall/fluid interface exhibits an uncertain boundary due to thermal oscillation, discrete nature, and intermolecular force penetration. The thermal oscillation of atomic scale interface may create a temperature dependency of boundary definition, which does not be considered in the continuum description. The discrete nature is the marked difference of atomic-level interface from the continuum description of the interface. In nanoscale, the discrete nature is dominant and the criterion to define the boundary between two dissimilar materials become unclear in this scale.

Moreover, the intermolecular force penetration throughout the interface allows a wall molecule transfer the energy a fluid molecule beyond their interface and vice versa, so that the molecular level interface is possible to be a thin space rather than a plane. Thus, the atomic scale interface is a complicated problem.

The uncertainty of the interface between the wall and fluid molecules is roughly an atomic diameter. This amount of uncertainty can be negligible in the continuum scale, and in that scale, the interface exhibits an apparent boundary (See Figure 1(a)). However, in a small system like the interior of Carbon Nanotubes (CNTs), one atomic diameter uncertainty may play a significant role in the accuracy of modeling because the boundary is coupled with the mathematical description of the physical property, dynamic property, and various issues in modeling. Moreover, as semiconductor production processes have been reduced to single-digit nanometer sizes [20, 21] and novel nanochannel fabrication techniques have emerged [22, 23], the molecular-level definition of wall/fluid interface has become a practical problem. Thus, an atomic-level definition of wall/fluid interface has to be fully clarified for accurate modeling of nanoscale physics.

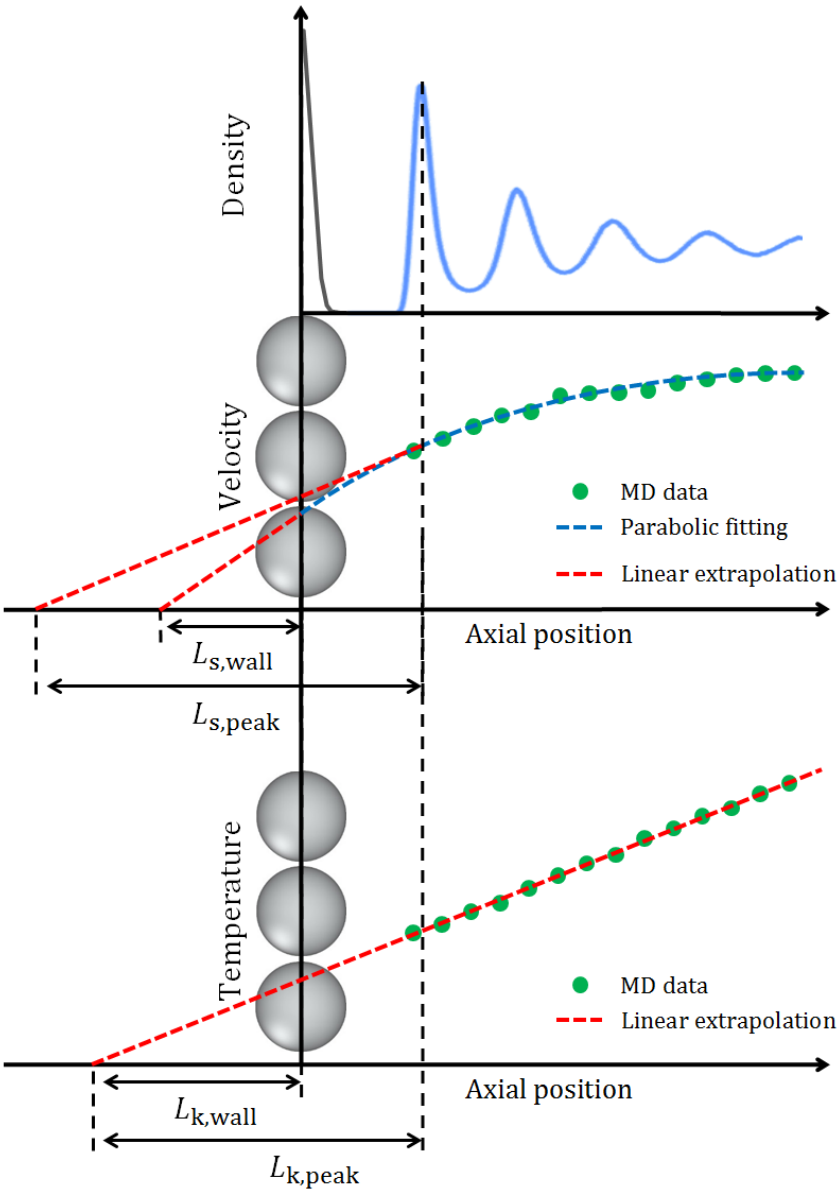

Figure 2. Determination of slip phenomena (a) velocity slip and (b) thermal slip

One of the problems induced by the atomic-level uncertainty of the current wall/fluid boundary definition occurs in the interfacial slip measurement process. It is well known that the velocity and thermal slip phenomena become non-negligible at about a 100

molecular diameter scale cause a significant deviation from the continuum mechanics. These slips are known to be originated from a non-perfect match between solid and fluid [24-26]. To understand these phenomena, intensive MD simulations were conducted during the past decades. Typically, the pressure driven flow creates a parabolic velocity distribution along the direction normal to the solid surface [27-31]. To measure the slip length, both linear and parabolic fitting have been used. Figure 2(a) shows the determination of velocity profiles in MD simulation using a parabolic fitting. It is evident that the solid/fluid boundary influences on this process. Similarly, during the thermal conduction through the solid-liquid entails the temperature discontinuity at the interface. It is verified that the temperature profiles of confined fluid during thermal conduction is linear for the channel is larger than ~ 10 molecular diameters [24, 32]. Hence, linear fitting is used to determine the thermal slip, which is also known as Kapitza length as shown in Figure 2(b). Obviously, based on the definition of boundary, the value of slip can be varied.

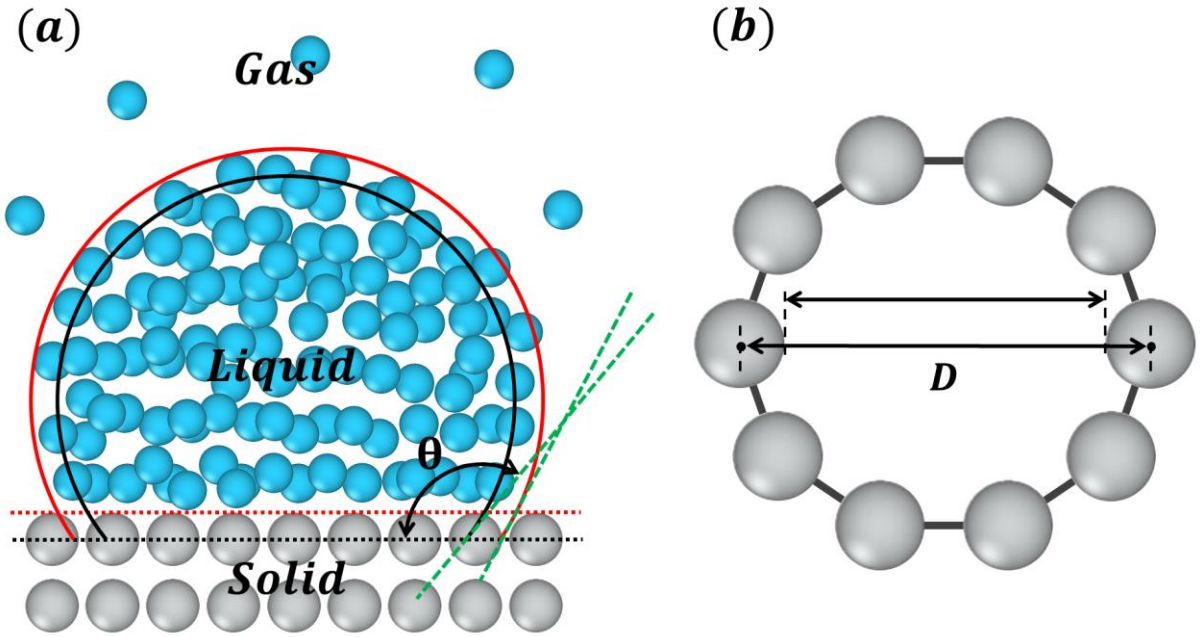

Figure 3. Determination of (a) the nano-contact angle and (b) diameter of nanotube at the molecular scale.

Not only the slip phenomena but also other measurements, such as contact angle, the diameter of a nanotube can also be affected by the boundary definition. The nano-contact angle measurement is one of a vital computer experiment to specify the solid/fluid interaction strength. Contact angle is related with the wetting behavior, and it also is known to be coupled with the interaction strength. As the interaction strength plays a crucial role in the interfacial phenomena [33-37], it is imperative matter in the MD simulation. As shown in Figure 3(a), the contact angle problem is related to two different interface (i.e. solid/liquid and liquid/gas). In addition to the contact angle measurement, determination of the diameter of a nanochannel is also essential step for analyzing the nanochannel. The diameter directly effects on the evaluation of the volume inside of the channel, especially in nanopore applications. Figure 3(b) represents the process for

determination of nanochannel diameter. As can be seen, the diameter of the nanochannel can be appreciably diverse depending on where the interface is set. The work done by Jiang *et al.* [4] utilized the electron density to determine the nanopore diameter. Similarity, a study done by Heiranian *et al.* [3] estimated the cross-section area of nanopore considering the diameter of individual atoms consisting of the pore.

The main problem caused by the absence of an atomic-level definition of the dissimilar boundary is that it can cause misinterpretations of nanoscale phenomena and thus lead to misunderstanding of nanoscale mechanics. Therefore, in the present research paper, the demonstrations of these problems were presented mainly, regarding thermal transport phenomena.

The boundary problem is also related to multi-scale analysis/simulation. The multi-scale theory uses implicit approach, which does not take into account the strict definition of dissimilar boundary. Nonetheless, if we specify and designate a proper boundary definition on the multi-scale method, it will greatly improve the current understanding of nanoscale physics and designing of various nano-devices. For multi-scale theory, there have been efforts to model nanoscale dynamics with classical continuum theory. In general, the classical continuum mechanics is partially applicable in nano-confined environment because of interfacial phenomena including structural inhomogeneity near the interface. For instance, Fourier's law is applicable to the channel larger than 3nm except at interface [12, 24, 32] and Navier-Stokes equation is valid in bulk region of nanochannel [19, 38, 39]. Based on those foundations, researchers have developed the modified continuum theories through boundary treatment for nano-confined liquid flow [39], viscous heating in nanoscale shear driven flow [40, 41], and the capillary rise of water in

nanotubes [36]. There is another stream called empirical potential-based quasi-continuum theories (EQT), which facilitates fast computations while keeping atomistic detail. This approach successfully predicted density variation near interface [42], fluid flow of Lennard-Jones fluid [31], its mixture [43], water [30] and even thermodynamic properties [44], for the confined environment.

The problems originated from the absence of a molecular-level definition of interface have been reported in the several pieces of literature. Nagayama et al. [27] documented that definition of wall/fluid interface affects the determination of slip length. In order to measure the slip length, they assumed that wall/fluid interface is located at first peak density, but the validity of the definition was not discussed. Similarly, Han et al. [45] noted that the definition of the interface at innermost solid layer induces a higher Kapitza resistance value than that at first peak density. Also, Kim et al. [41] demonstrated that the definition of wall/fluid boundary affects local property calculation near the wall and pointed out that the center of the innermost solid layer is not the exact boundary between solid and liquid, but the area occupied by the solid molecules. Their finding has supported this idea that the local viscosity adjacent to the wall can be calculated more accurately when the volume occupied by solid molecules is excluded. In addition, it has been reported by Ramos-Alvarado et al. [13] that the definition of wall/fluid and liquid/gas interface should be clarified for precise measurement of the contact angle of nano-droplet. To solve the problem, they defined the boundary at locations corresponding to the half bulk density of droplet. However, the physical meaning or validity of the definition was not documented. As several studies have reported, a proper definition of the atomic-scale interface is necessary for the better understanding of nanoscale physics and thus for accurate modeling of nano-devices. Despite many studies, the definition of wall/fluid

interface varies from researcher to researcher. According to our literature study, the definitions of interface used by researchers are mainly classified into four categories: I) innermost wall layer [14, 46-49], II) midpoint between the innermost solid layer and the first peak density [45, 50], III) First zero density of liquid layering (~ an end of tail of adsorption layer) [30, 51], IV) First peak density (~ one molecular diameter spacing from innermost wall layer) [39, 52-55]. These different definitions of wall/fluid boundary have created quantitative and even qualitative discrepancies, which hinder understanding of nanoscale physics. However, little attention has been paid to the atomic-scale definition of wall/fluid interface.

The present study was designed to demonstrate errors due to the various definitions of an atomic-level interface, and discuss its seriousness. The rest of the article is organized as follows: In section 2, we provide the simulation details. The later section discusses local thermodynamic equilibrium near the interface, thermodynamic property, material property, and scale effect of boundary effects. Finally, a summary of results and future research are presented. This work would be a cornerstone of a molecular-level definition of the interface.

2. Theoretical Background

2.1. Introduction of theoretical background

The innovative idea came up by Ludwig Boltzmann that macroscopic phenomena must be reproduced from one fundamental principle is the cornerstone of statistical mechanics and thus Atomic simulation including MD simulation. The classical statistical mechanics is one of the essential theory to bridge the gap between motional information obtained from MD simulation and macroscopic properties, which is empirically defined by earlier scientists. The classic statistical mechanics describe the microscopic features with the complicated mathematical descriptions, which is nearly impossible to be solved analytically. This was a major limitation of statistical mechanics until the computer was developed. The computer can numerically solve Newton's equation of motion of the molecules and thus to get all atomic trajectories. Even though the atomic trajectories obtained from MD simulation normally deviate from actual trajectories soon after simulation starts, the aggregations of motional information, which is called ensemble average, can be converted into empirically defined properties via statistical mechanics, linear response theory. Investigation of thermodynamic properties using molecular dynamics simulation was initiated by the pioneering works by Verlet [11] around 1967. It has been verified in various literature for many years. Furthermore, this computer experiment has been successfully extended to investigate dynamic properties, material properties. More recently, intensive studies have been conducted on the interfacial phenomena such as momentum slip, interfacial thermal resistance, electric double layers,

and structural inhomogeneity near the interface. In the following text, several theoretical foundations to evaluate thermodynamic properties near the wall/fluid interface used in Molecular Dynamics simulation are presented.

2.2. Ergodic hypothesis

Because MD simulation is computationally demanding, it is typically performed in the limited scale of time (~100 ns) and space (~100 nm). Due to these technical limitations, MD simulation typically handles a continuum scale system. Under the limited number of atoms, there is a question about the statistical significance of MD simulation [56]. The statistical significance must be maintained to use statistical mechanics for data processing of molecular trajectories. In addition to the limit of MD simulation, to investigate microscopic phenomena, we need to investigate very small areas. For example, one important step to study thermal transport phenomena along the nanoscale liquid film is determining the temperature gradients of the liquid film. The process to measure the temperature gradient in MD simulation necessarily entails defining the local temperatures in a very small area (~Å) or even smaller areas where the statistical significance may not be guaranteed [24]. Likewise, investigating the nanoscale phenomena using MD simulation need to show the statistical significance. For these reasons, it is important for MD simulation to employ Ergodic hypothesis. According to the Ergodic hypothesis, for the random process, ensemble average can be replaced by the time average. Generally, MD simulation is a highly random process. Accordingly, the MD simulation is usually permitted to use data collected along the time axis as well as space axis. By using two directional data (i.e. time and space), we can get as much available data as the product of

data correcting time and local space for data processing. In that case, by increasing the data collection time, we can increase the likelihood of ensuring statistical significance in MD simulation. Based on our investigation of the statistical significance and data collection time, 2ns data collection time in a small segment where averagely ten atoms exist during equilibrium state is enough to maintain the statistical significance.

2.3. Local Thermodynamic Equilibrium (LTE)

Even if data are collected over a long time, the statistical significance might not be ensured in extreme conditions such as adsorption layers and superfast transport in None-equilibrium Molecular Dynamics (NEMD) simulation. If the statistical significance of a local system is not ensured, the property evaluation with statistical mechanics is meaningless. Therefore, it is desirable to show the statistical significance of data obtained at the local segment when NEMD simulation is performed.

The Maxwell-Boltzmann distribution is derived on the assumptions of ideal gas and thermal equilibrium. This distribution is mathematically described as follows:

$$\mathrm{f}(v_i) = \left(\frac{m}{2\pi k_B T}\right)^{\frac{3}{2}} \exp\left\{-\frac{m}{2k_B T}\left(v_{ix}^2 + v_{iy}^2 + v_{iz}^2\right)\right\} \tag{1}$$

The shape of the Maxwell-Boltzmann distribution depends on the temperature and atomic mass (material) as depicted in Figure 4. When the temperature increases while atomic mass is fixed, the speed distribution becomes a flat shape as well as the average speed increase. On the other hand, when the atomic mass increases with constant

temperature, the form of distributions become sharp. A system that satisfies the Maxwell-Boltzmann distribution also satisfies that each component of velocity follows a normal distribution and thus has zero mean velocity (i.e. $\sum_{i=0}^{n} v_i = 0$). In addition, the important point of Maxwell-Boltzmann distribution is that the fluids in equilibrium state follow this distribution. Based on this fact, it is possible to confirm whether the local equilibrium is satisfied by comparing the velocity distribution with the normal distribution or speed distribution with the Maxwell-Boltzmann distribution. Also, it is possible to quantify this by calculating the correlation factor between the obtained velocity distribution from MD simulation and theoretically driven Maxwell-Boltzmann distribution.

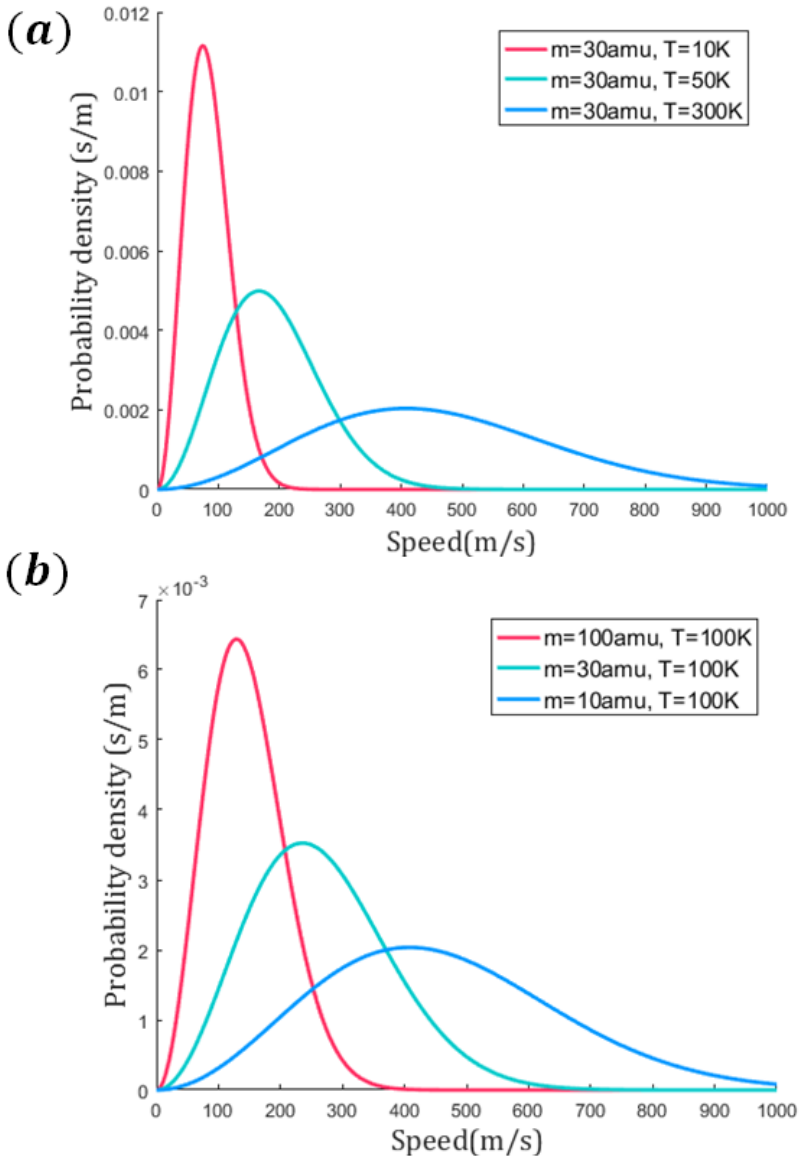

Figure 4 Maxwell Boltzmann distribution with respect to (a) temperature and (b) Atomic mass.

2.4. Microscopic description of Temperature

Temperature has several definitions with respect to the point of views. The macroscopic view of temperature is a potential to transport thermal energy. According to

this description, thermal energy flows from high temperature (i.e., high potential) to low temperature (i.e., low temperature). This description gives valuable insights into the concepts of temperature. The continuum thermodynamic describes temperature as the rate of increase of entropy with energy for a pure substance, $\frac{1}{T} = \left(\frac{\partial S}{\partial E}\right)_{NV}$. Where s is entropy and E is energy. The MD simulation typically adopts the microscopic description of temperature to evaluate temperature. As is well known, the average kinetic energy is proportional to the absolute temperature. According to the kinetic theory, the temperature is mathematically described as follows:

$$\mathrm{T} = \frac{2}{3Nk_B}\langle E_k \rangle \tag{2}$$

Where N is number of atoms in the corresponding region, k_B is Boltzmann constant, and E_k is kinetic energy in the corresponding region. This mathematical description is derived from the assumption of ideal gas and may not be applicable to liquids or solids, which totally violate idea gas assumption. Despite of the disagreement in the assumption, the fundamental description of temperature for a pure substance, $\frac{1}{T} = \left(\frac{\partial S}{\partial E}\right)_{NV}$, yields the identical mathematical expression for liquid and solid [57] in the microcanonical ensemble. Therefore, it is possible to estimate temperature using the Eq (2) regardless of the phase of material in the MD simulation with the microcanonical ensemble.

2.5. Microscopic description of Pressure

Physically, pressure can be explained by the momentum flux carried by atomic mass (kinetic contribution) and transferred by interatomic force (configurational contribution) [57]. Also, thermodynamic definition of pressure is described as a normal force per unit area to maintain a certain volume in a constant mass and temperature system, which mathematically described as: $P = -\left(\frac{\partial F}{\partial V}\right)_{N,T}$. These two different explanations of pressure can be used in MD simulation to compute pressure and it yields nearly identical consequence [58]. In the present study, the physical route is utilized to estimate pressure. The microscopic expression of pressure tensor is described as follows:

$$P = \frac{1}{3V}\left(2N\langle E_k\rangle + \langle W\rangle\right) \tag{3}$$

Where N is the total number of atoms, $\langle E_k\rangle$ is an ensemble average of the kinetic energy, $\langle W\rangle$ is an ensemble average of the virial. The kinetic contribution to pressure is identically described regardless of material or state, as in the case of temperature. On the other hand, the virial contribution is expanded to the complicated expression in case of the complex materials, surface geometry [57], and periodic boundary condition [59]. In this study, as the Lennard-Jones monoatomic fluid is employed the virial contribution is expressed in a relatively simple form as follows:

$$P = \frac{1}{3V}\left(2N\langle E_k\rangle + \sum_{i}\sum_{<j} \mathrm{F_{ij}} \cdot \mathrm{r_{ij}}\right) \tag{4}$$

Where F_{ij} is an interatomic force vector between i and j atoms and r_{ij} is a relative positional vector from i to j atom.

2.6. Interatomic potentials in MD simulation

An important first step to perform MD simulation is to specify a proper interatomic potential. The Lennard-Jones (LJ) potential is popular and intensively studied during the past few decades. This potential mathematically represented as follow:

$$U(r) = 4\varepsilon\left(\left(\frac{\sigma}{r_{ij}}\right)^{12} - \left(\frac{\sigma}{r_{ij}}\right)^{6}\right) \tag{5}$$

Where ε is the depth of the potential well, σ is the molecular diameter, and r_{ij} is the intermolecular distance. This potential is simple but powerful to represent the molecular behavior of fluid flow and heat transfer. When two atoms are at a distance closer than the atomic diameter, σ, this potential acts like a soft ball and pushes them apart. This term is represented as the 12 power in the Eq. 5. However, when the molecules are at a distance far from the molecular distance, the molecules pull together with weak force, which mimics the Coulomb interaction. This potential approximation is not perfect, but it can reproduce the bulk behavior of the molecules by adjusting the parameters appropriately. For this reason, LJ parameters have been studied for argon, which is a singlet inert gas. The results of the LJ argon have shown good agreements in both theoretical prediction and experimental measurements [24, 26, 47, 60-64]. For actual MD simulations, Truncated LJ

potential is usually used to reduce the computational costs. The truncated LJ potential mathematically describes as:

$$U_{\text{truncated}}(r) = 4\varepsilon\left[\left(\left(\frac{\sigma}{r_{ij}}\right)^{12} - \left(\frac{\sigma}{r_{ij}}\right)^{6}\right) - \left(\left(\frac{\sigma}{r_c}\right)^{12} - \left(\frac{\sigma}{r_c}\right)^{6}\right)\right] \quad (6)$$

Where r_c = 1 nm is the cut-off distance. It is known that the cut-off distance is known to be closely related to the mean free path of the system. The cut-off distance should be at least longer than the average free path, and three times or more is recommended. The cut-off distance has a negligible effect on the ensemble average of the system when three or more molecular diameters of the cut-off distance is determined.

To model metallic systems in MD simulation, Embedded Atom Model (EAM) potential is widely used. The EAM potential can reproduce experimental and first-principles data such as lattice constant, elastic modulus, cohesive energy, phonon frequencies, thermal expansion coefficient, melting temperature, and lattice-defect energies [65-67]. This potential well reproduces the metallic parameters; however, the combined use of EAM with LJ potential for solid and fluid respectively yields an unrealistic mismatch. Vo *et al.* reported during the study of silver melting interface that the EAM/LJ interface have an inherent mismatch [25]. EAM potential and LJ potential are not perfectly compatible with each other, but due to their merits, solid/fluid systems using these two have been actively studied [60, 68-72].

2.7. Ensemble averages for MD simulation

The molecular ensemble is a key concept in statistical mechanics, which is one of the cornerstones of MD simulation. Unlike the classical thermodynamics, the statistical mechanics uses microscopic states of the system to reproduce its properties. The microscopic states widely used in the MD simulation are Microcanonical Ensemble (NVE), Canonical Ensemble (NVT), and Isothermal-isobaric ensemble (NPT).

The NVE ensemble constrains the number of particles in the system, the system volume, energy, which mimics an isolated system. Although isolated systems are hardly implemented experimentally, NVE ensemble is considered the most realistic microscopic state. In MD simulation, NVE ensemble is achieved by solving equations of motions of all particles by maintaining constant internal energy, which is determined by initial velocity distributions, configurations of atoms. As a result, the NVE ensemble allows the temperature to slightly fluctuate during an equilibrium state. NVE ensemble can be utilized to investigate a coupled mechanism between fluid flow and heat transfer because it does not artificially control the temperature. Also, The NVE ensemble is recommendable to be utilized for static properties as well as dynamic properties. However, it is difficult to fix the system in a specific state during the NVE integrations.

The NVT ensemble fixes the number of atoms, the system volume, and the temperature of the total system. Unlike NVE ensemble, it does not allow the temperature to fluctuate. To maintain system temperature constant, it utilizes a thermostat, which manipulates the velocity of atoms (i.e., kinetic energy). Thus, this ensemble describes an isothermal condition and is considered similar to the general laboratory setting. This

enables us to easily investigate static properties at a thermodynamics state while this ensemble is not recommended to investigate dynamic properties. In addition, this method is very suitable for adjusting a system temperature, so it is usually used to reach a specific state at the beginning of the MD simulation and is commonly used in combination with the NVE ensemble.

NPT ensemble maintains the number of molecules, pressure, and temperature constant. To achieve it, this ensemble uses barostat and thermostat. The barostat works by adjusting the system volume. Manipulating pressure with this mechanism entails reaction time. This volume manipulation mechanism is suitable for fluidic systems that have homogeneous distribution. However, use in solid-fluid systems or solid systems may not be appropriate, and appropriate precautions are required before using it. In fact, the barostat mechanism does not work correctly in heterogeneous systems. Nevertheless, this mechanism is useful when used with caution, since it can easily manipulate thermodynamic states.

3. Methodology

3.1. Methodology Introduction

To elucidate wall/fluid boundary, three distinctive set up of MD simulations were considered: A) Equilibrium Molecular Dynamics (EMD) simulation for homogeneous liquid argon system B) EMD simulation for silver-argon nanoconfinement (constant T,P,v). C) Heat transfer MD simulation for nano-confinement. For all these simulations, Large-scale Atomic/Molecular Massively Parallel Simulator (LAMMPS) [73] was utilized and Open Visualization Tool (OVITO) [74] is used for the visualization. All simulations adopted the following atomic parameters. Lennard-Jones(LJ) potential was used for argon-argon interaction and silver-argon interaction with 10Å truncated distance, which is large enough not to disturb the systematic condition. The specific argon-argon and argon-silver inter-atomic potential were parameterized by Shi et al. [60]. The atomic mass of silver was set 107.8682 g/mol, and that of argon is 39.948 g/mol. For the modeling of solid silver, the Embedded Atom Model (EAM) potential is utilized.

3.2. EMD simulation for homogeneous system

A simulation was performed on a system consisting of homogeneous LJ argon to obtain a bulk property. The system is designed on a cubic box with 84.427Å length each direction, which is ~20 times larger than the mean free path of the liquid argon. The periodic boundary condition is applied to all directions to remove the finite-size effect.

The cube contains 12,195 Argon atoms as depicted in Figure 5, which number corresponds to the normalized density, ρ^*, of 0.800 in the cubic volume. The temperature controled by Nose-Hoover thermostat to maintain a target temperature of 100K, which thermodynamic state is liquid according to the LJ argon phase diagram [54, 75]. To calculate thermal conductivity, we use Green-Kubo relation [76, 77], which has been validated by several studies [12, 78]. NVT (Canonical) ensemble is performed during 4ns with 1fs time step for equilibrum at 100K temperature. After that, NVE (Microcanocical) ensemble was conducted for a total of 12ns. Among 12ns, 2ns is used for equilibration and 10ns is for data collection. The 10ns data collection is relatively long time given the typical data collection time is 2ns. The long data collection time alleviate statistical uncertainty of property calculation. The data obtained in this simulation used as the actual property of LJ argon utilized in the present work and compared with the confined property.

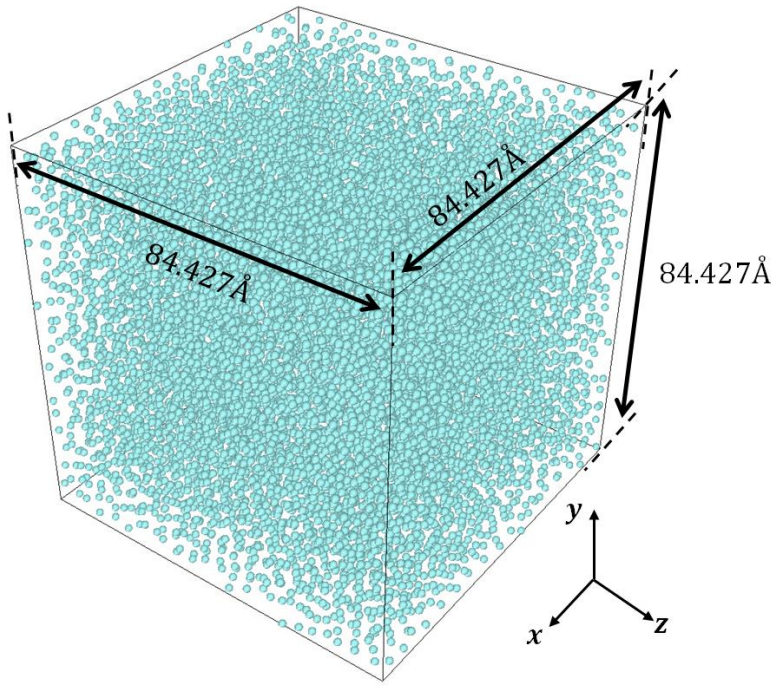

Figure 5 Simulation domain of the homogeneous argon cubic system.

3.3. Equilibrium MD simulation for nanoconfinement.

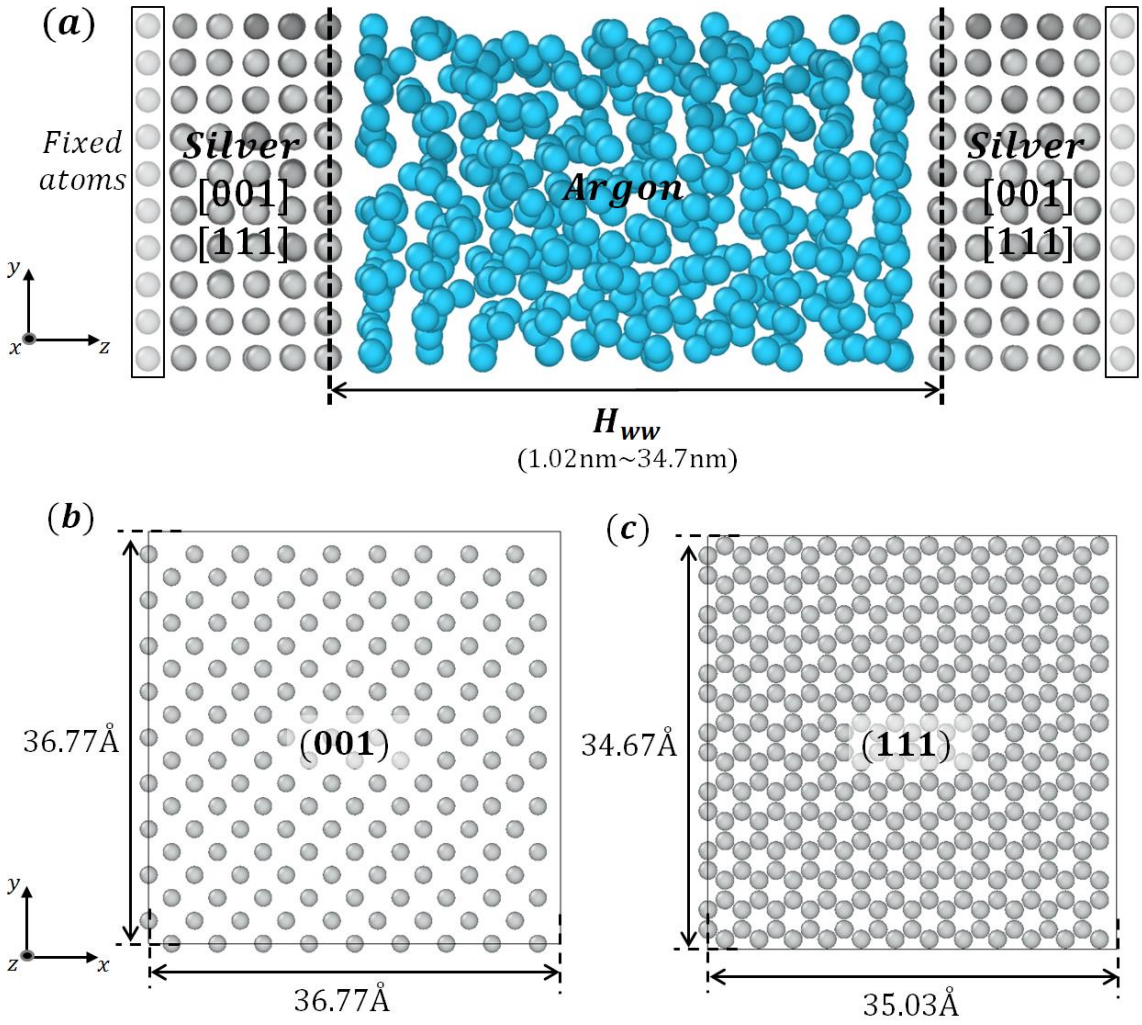

Figure 6. Graphical representation of the simulation domain for the nanoconfinement: (a) lateral view of the simulation domain, (b, c) initial Ag crystal setting for periodic boundary condition and different orientations.

MD simulations were conducted at an approximately identical thermodynamic state in order to study the local variation of property of the different sizes of nanochannel. The

size of the simulation box is presented in Figure 6(a). The sizes of the channel, H_{ww}, is ranging from 1.02nm to 34.7nm, which is correspond to the lenth scale of $3\sigma_{Ar}$~$100\sigma_{Ar}$. Two different crystalline orientations of (001) and (111) were considered as the contact surface of silver to the liquid argon in order to investigate the effects of crystal orientations on boundary definition. The periodic boundary condition is applied to x and y-direction and fixed boundary condition on z-direction for the constant channel heights during the equilibrium state. It is noted that the system domain must be carefully designed for periodic boundary condition. To properly design the periodic nanoconfinement, the system domain should be periodic patterns as dipicted in Figure 6(b), (c). The molecules at the outmost layers were not thermostated but fixed and the rest of molecules was thermostated to maintain 100K. For a proper comparison of different sizes of channel, it is essential to maintain a same thermodynamic state of the channel. However, due to the high inhomogeneous nature of the confined fluid, it is challenging to ensure an identical thermodynamic state, especially for the nanochannel that has no bulk region. To ensure the approximately identical thermodynamic state for the differences sizes of channels, the bulk density was adjusted to be 0.8 at the large channels, and the first peak location, which is affected by the temperature and pressure in nanoconfinement, was adjusted to be about 2.83 for (001) and 2.89 for (111) for all channels including the small channels where no bulk region exist. These processes were done through trial and error to change the number of fluid molecules. The first 2ns is integrated by NVT ensemble for the equilibration at 100K and NVE ensemble was performed for 3ns. The first 1ns is used for equilibration and rest 2ns is for data collection. In fact, the NVT ensemble can be used to estimate a thermodynamic property at the confined environment, we use NVE ensemble for the thermodynamic property for more physically reliable data.

3.4. Heat transfer MD simulation

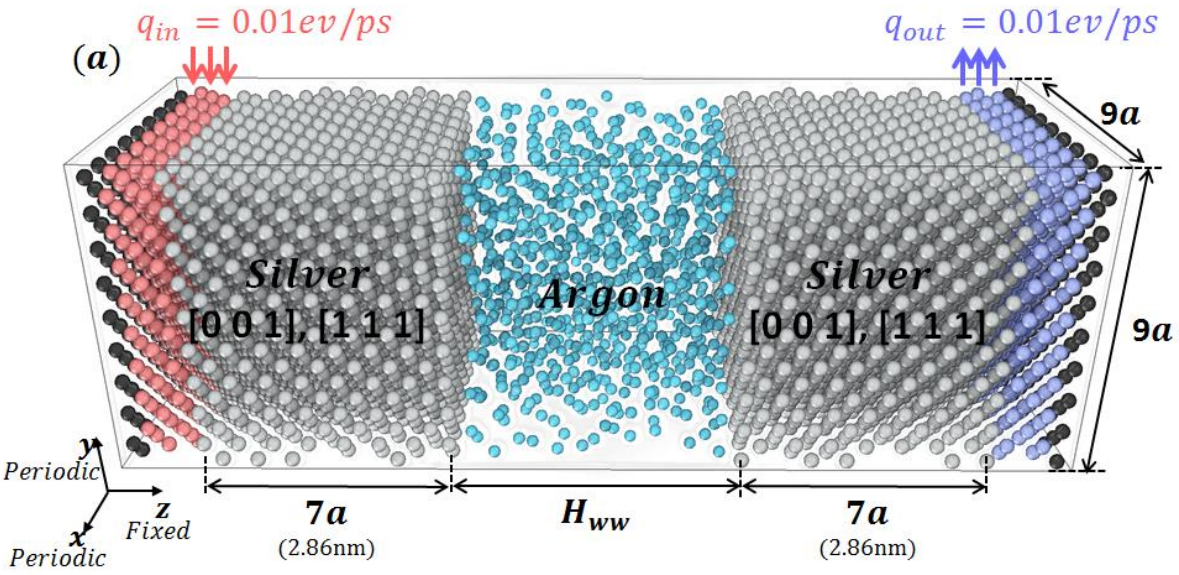

Figure 7. Pictorial representaion of simulation detail for the heat transfer MD simulation.

Non-Equilibrium Molecular Dynamics (NEMD) simulations were conducted to elucidate wall/fluid interface through the perspective of heat flux and thermal conductivity as shown in Figure 7(a). The simulation domain were $9a \times 9a \times (14a + H_{ww})$ except fixed layer and thermostated layers. Three different sizes of channels, H_{ww} = $3.47nm, 10.42nm, 34.73nm$ and two different contact orientations, (001) and (111) of FCC silver, were considered. There are 15 silver layers between the thermostated layer and liquid region, which is substantially alleviate the effects of a number of solid layers on Thermal Boundary Resistance (TBR) [79]. The periodic boundary conditions were applied to the x and y directions and the outmost Ag layers were fixed to maintain a specific channel height and thus a constant volume during the equlibrim state. To appropriately apply the periodic boundary condition to these directions, the system domain of x and y

coordinates should be enough to reduce the finite size effects along the direction. Typically, it is recommended to utilize the length scale that is larger than the phonon mean free path of the material. Nonetheless, we use 9 lattice constants for the computational efficiency, which is smaller than the phonon mean fress path of the silver because our purpose on this simulation is mainly focused on the heat transfer at solid/fluid interface. The outermost second to fourth layers were thermostated, which manipulate the velocity magnitude into conserving aggregate momentum. 0.01ev/ps heat is produced in the left thermostat and this amount of heat is removed from the right thermostated layer. Thus, averagely 0.01ev/ps heat is transferred through the z-direction of the channels during the steady state. The MD simulation was performed under NVT ensemble during 2ns to equilibrate the system at 100K. After NVT ensemble, NVE ensemble was activated during 24ns with two local thermostats. The first 14ns is for equilibration to reach steady state heat transfer and 10ns is for data collection, which is sufficient to obtain reliable statics.

We noted that the NPT ensemble (Isothermal - Isobaric) was not utilized in the present work although some works on wall/fluid nano-confinement were conducted in the NPT ensemble [79-81]. The sole use of NPT ensemble can obscure the close investigation of boundary because its barostat algorithm cannot fully reproduce the nature of heterogeneous systems [55]. Also, NPT-NVE has a mismatch at the ensemble transition. This mismatch between NPT and NVE ensemble induces an uncertain volume in the NVE ensemble, which depends on the last time step of NPT integration. Since the pressure in the incompressible system is very sensitive to the volume, a combination of NPT and NVE is inadequate for the nanoconfinement. Therefore, we use NVT-NVE sequence, which shows a good ensemble transition.

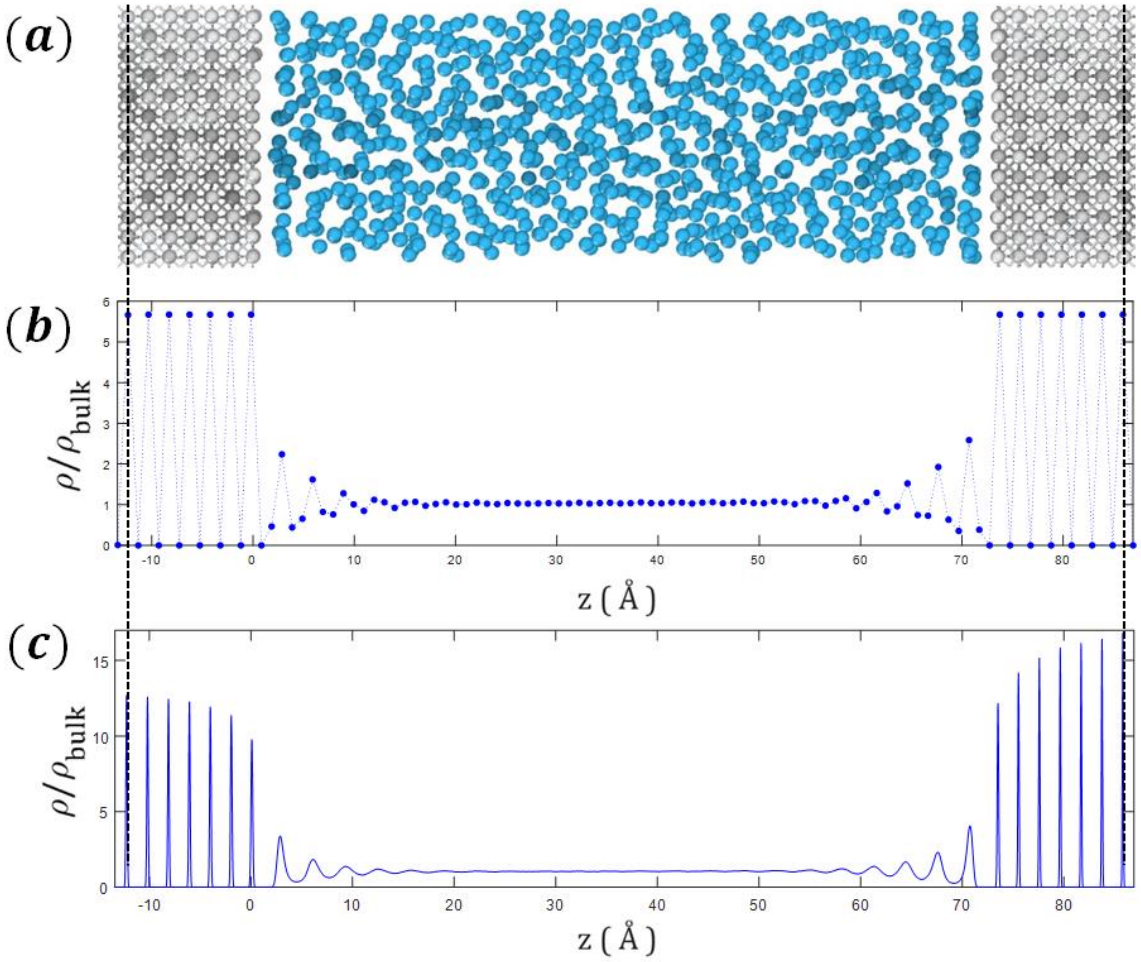

Figure 8. Density distributions of two different bin size: (a) simplified system domain (b) bin size of 1/4 atomic constant and (c) fine bins.

To investigate the confined system, it is necessary to obtain the local variation of properties. This process is done by binning the system into several part and converting the data into the macroscopic property such as temperature, pressure and heat flux. There is no rigorous way to define the bin size for it, mainly two methods are recommendable. The first way is to divide the bin considering the solid lattice constant as shown in Figure 8(b) [82]. This method is useful to determine the system structure with reliable statistics in a short running time. Therefore, it is recommendable to use this method for the solid system

or large system. Another way is to divide the bin finely to display a full resolution of the system. This method is computationally expensive though it has some advantages. Firstly, it well distinguishes the differences between solid and adsorbed fluidic structure. Also, it contains the information of thermal vibration at both in the solid and confined fluid. Especially for the solid, it appears to determine the temperature only from the density distribution. Figure 9 shows a clear relation between the temperature and density distribution. It is obvious that the probability distribution of an atom in absolute zero temperature follows delta function when we assume the atomic mass is concentrated at the center of the atom. However, as the temperature increase, the thermal vibration of an solid atom displays a bell shape distribution, which depicted in the subfigure of Figure 9. This process only possible when we observe the full resolution of density distribution using fine binning.

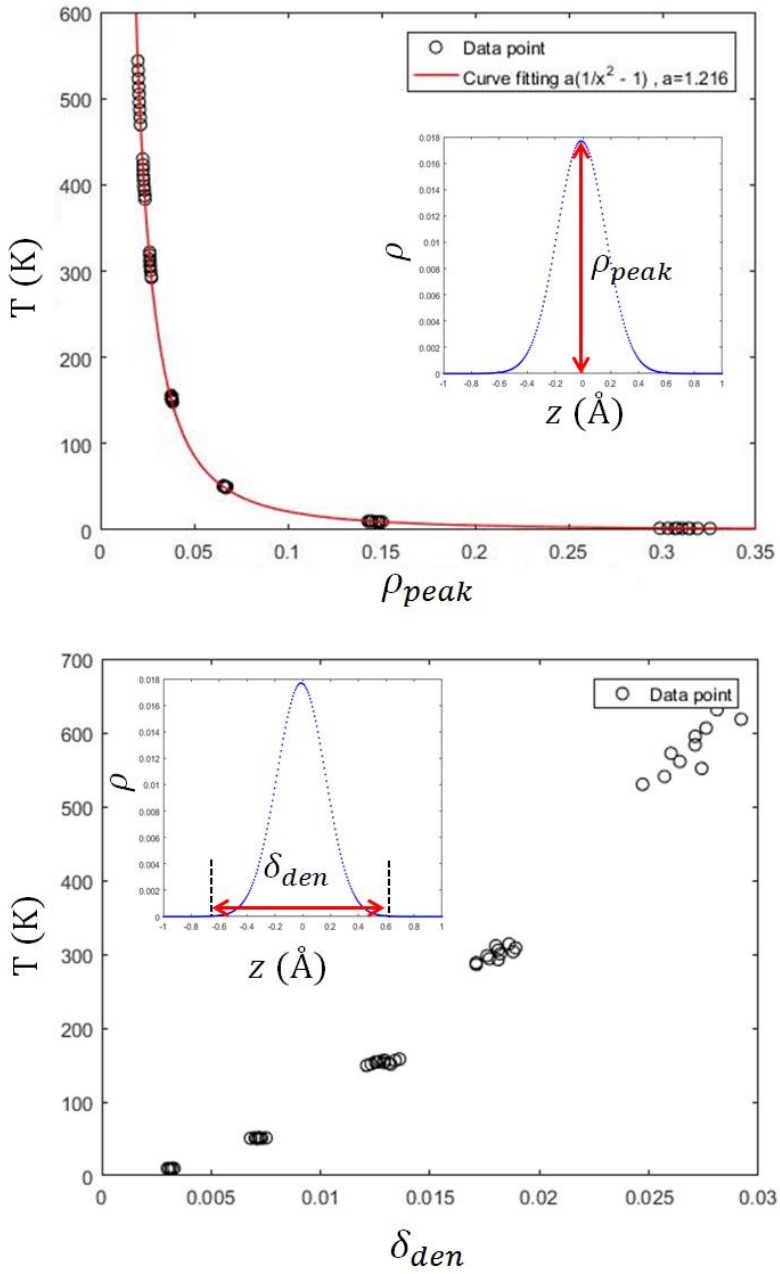

Figure 9. Relations between temperature and probability density distribution of solid obtained by MD simulation.

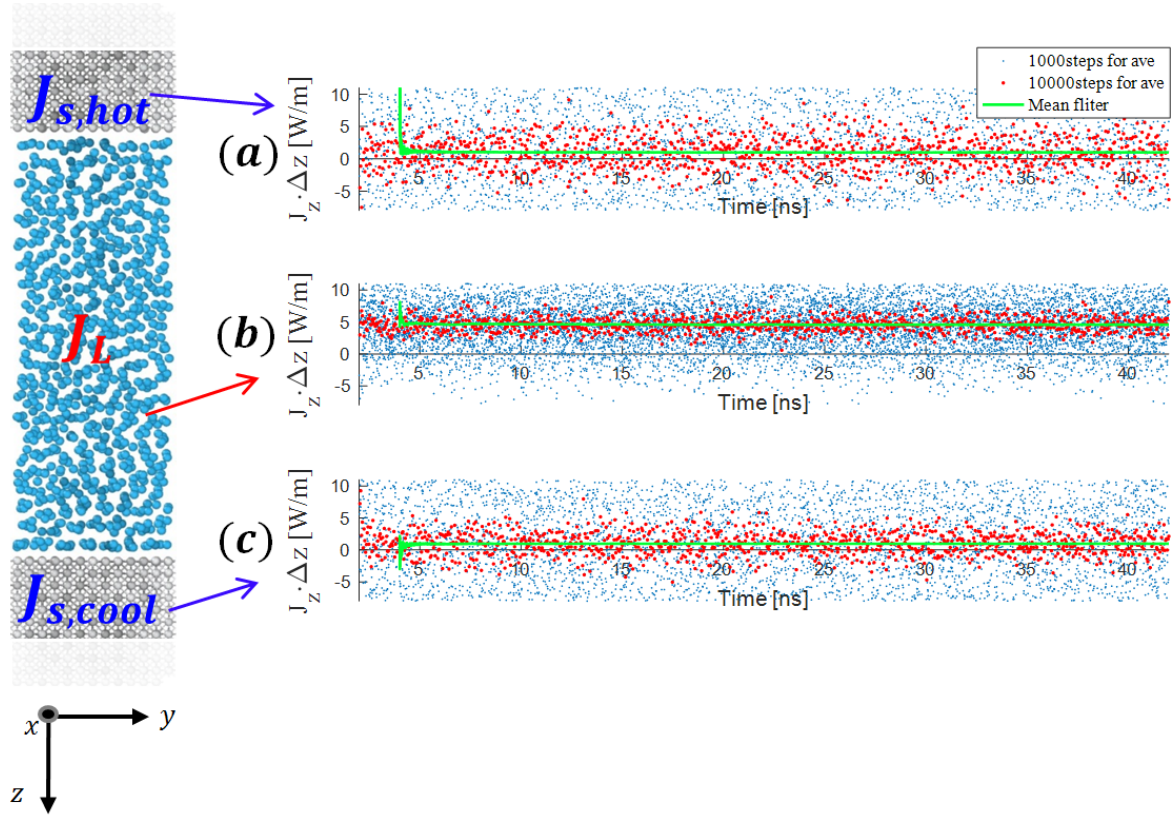

Figure 10. The fluctuations of heat flux calculation at (a) the high-temperature silver region, (b) confined argon and (c) low-temperature silver region

It is apparently important to ensure the reliable statistics for all property calculation. The heat flux calculation entails the complicated calculation. For this reason, the heat flux calculation takes a relatively long time to ensure the statistical significance. Figure 10 shows the fluctuations of heat flux data collected from the MD data. Even though we utilize long data collection time (40ns), the heat flux data still fluctuate. In this case, the mean filter is used to estimate a reliable heat flux data. The solid green line in Figure 10(a-c) is the filtered data using a mean filter. As can be seen, after 5ns, the fluctuations of the heat flux are alleviated within the reliable errors. Thus, we use the mean filter for the heat flux calculation.

4. Results and Discussion

4.1. Defining terminologies

Before getting into the details of the results, we clarify some terms. Figure 11 illustrates the terminologies used in this work with typical stress and density profile in a confined environment. For the density and stress profile, we assumed that an atomic mass is concentrated at the center of an atom, which is referred to as a center point mass concept. The bin size is selected to be fine enough to observe the smooth resolution and to maintain statistical significance. The term 'Innermost solid layer' was defined as the most probable location of the innermost solid layers, and this location is aligned at $z = 0$ in this study.

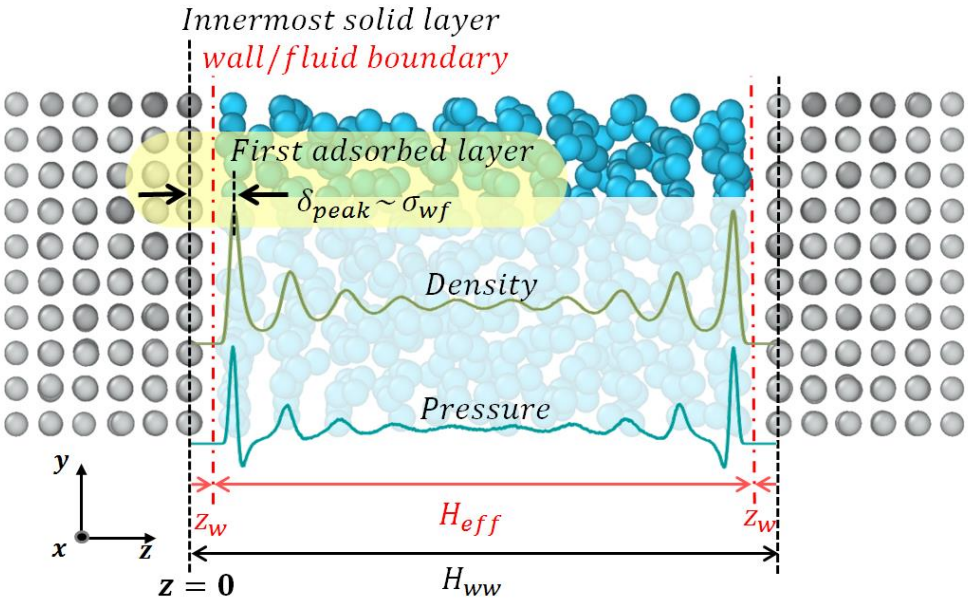

Figure 11. Pictorial explanations of terms used in the present study

The term ‘first adsorbed layer’ was defined as the location corresponding to the first peak of liquid layering. The wall/fluid boundary is the provisional definition of wall/fluid interface. The variable, z_w, indicates a distance between the innermost solid layer and the wall/fluid boundary. We examined several properties by shifting the boundary definition from the innermost solid layer to the first adsorbed layer. The wall to wall width, H_{ww}, was defined as the distance between two innermost solid layers. The effective channel height was defined as $H_{eff} = H_{ww} - 2z_w$ by considering the atomic-level boundary definitions. Gap distance, δ_{peak}, was defined as a distance between the innermost solid layer and First peak density. The gap distance is known to be closely related to the interface phenomena [14, 52, 83, 84].

4.2. Investigation of local thermodynamic equilibrium

Before close investigation of molecular-scale wall/fluid interface, the local thermodynamic equilibrium was investigated to confirm the validity of local properties near interface by comparing the speed distributions obtained from MD simulation with the Maxwell-Boltzmann distribution. The local equilibrium was checked at the slab bin with a width of 0.05Å (See Figure 12), which is small enough to capture the full resolution of the structural inhomogeneity. Each corresponding velocity data inside of bin were collected during 200ns, which is relatively long time considering that typical data acquisition time is 2ns. In Figure 12(a), it is shown that the region, $0 < z < 0.1\sigma_{wf}$, can be occupied by the center of silver molecules due to its thermal motion. At the approximately end of the thermal oscillations of solid layer (i.e. (b) and (c) in Figure 12), the statistical significance is drastically broken. The correlation coefficient, R, indicates how well the simulation data

are matched with Maxwell-Boltzmann distribution; the value $R = 1$ indicates perfect match and $R = 0$ imply no correlation. Figure 12(b) represents velocity distribution obtained by MD simulation at the segment and the corresponding Maxwell-Boltzmann distribution. The two distributions are matched almost perfectly indicating 99.99% correlation. On the other hand, the Figure 12(c) has 98.53% correlation, which location is just 0.1Å from the location of (b). Also, the local thermodynamic equilibrium at the adsorbed argon layer is examined. Figure 12(d) shows a very good agreement with the ideal speed distribution while Figure 12(e) shows a relatively pool agreement. Comparing the velocity distributions at solid sliver and fluid argon, the silver region shows a sharper speed distribution than those of argon. When we assume that the statistical significance is broken on the basis of 99% correlation, the local thermodynamic equilibrium was broken at approximately $z_w = 0.1\sigma_{wf}$ and $z_w = 0.75\sigma_{wf}$. Hence, in this case, it is impossible to define local property between $0.1\sigma_{wf}$ and $0.75\sigma_{wf}$ from a statistical point of view with the center point mass concept. We name this area as a statistical depletion region. The center of both silver and argon atom cannot reach to the region (i.e. $0.1\sigma_{wf} \leq z_w \leq 0.75\sigma_{wf}$). However, it may not mean a totally empty region, but the zero density area is occupied by electrons in reality. The statistical depletion region can vary with the thermodynamic states and molecular characteristics because this region is closely related with the density distribution. A further investigation into the statistical depletion area would be necessary to bridge the gap between the continuum theory and the discrete-scale dynamics. To deal with this matter, quantum based simulation would be necessary.

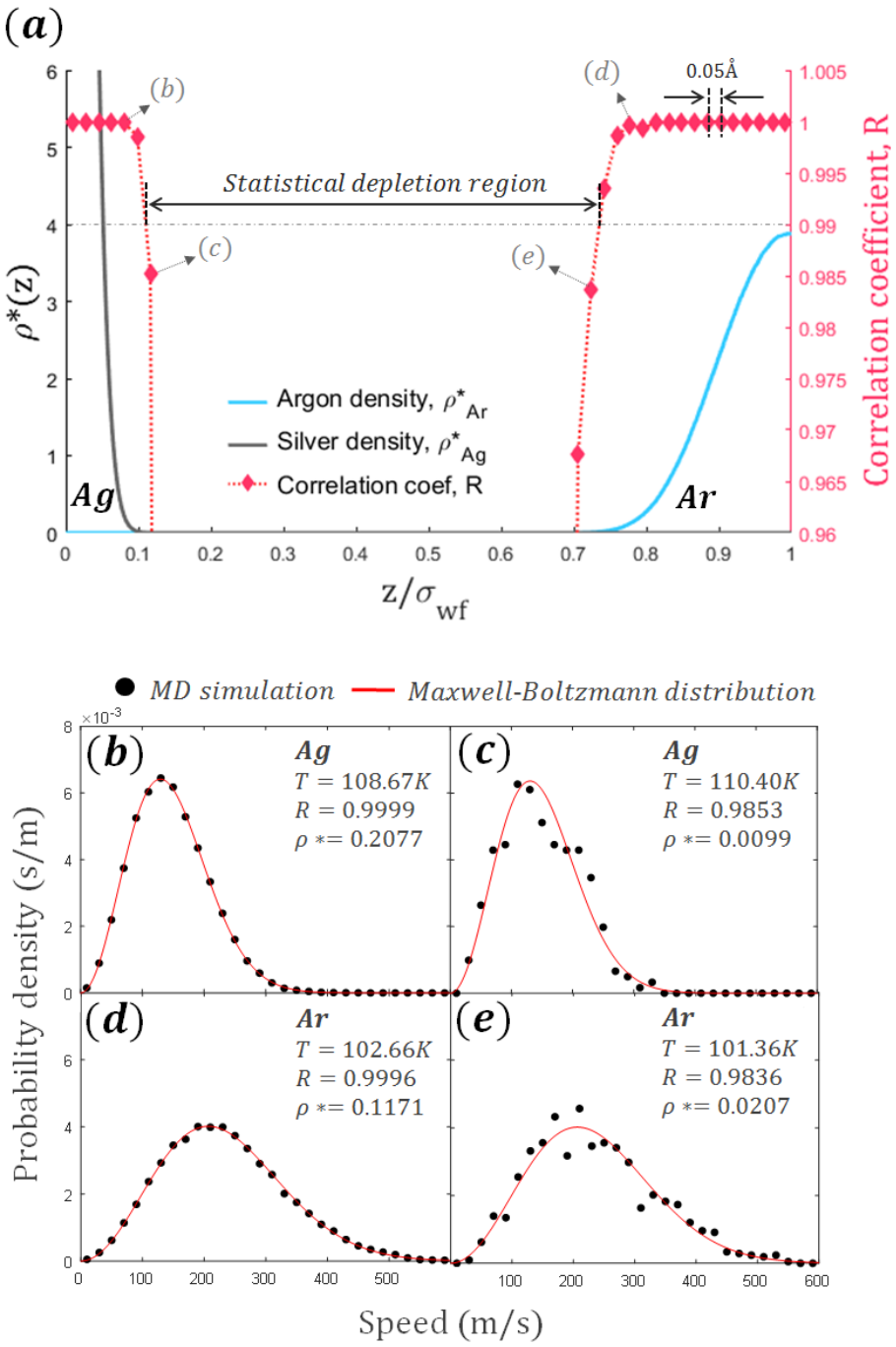

Figure 12. Statistical validity near wall/fluid interface. (a) Density and correlation coefficient along z-direction. (b-e) Normalized speed distribution obtained by MD simulation and the Maxwell-Boltzmann distribution at corresponding temperature. The interval of MD simulation is $20\mathrm{m/s}$. The superscript, $*$, denotes the Lennard Jones dimensionless number.

4.3. Thermodynamic state of nanochannels

After check the statistical significance of the local properties, we compare the thermodynamic properties obtained from different methods. In Table 1, we summarized the thermodynamic properties of argon. The homogeneous LJ Argon system shows a good agreement with the the bulk region confined LJ Argon. Also, the thermodynamic proeprties of argon via experiment conducted by Tegelar et al [85]. is in agreement with those obtained from MD simulation. Therefore, the argon potential we utilize is considered reliable.

Table 1. Thermodynamic properties of argon obtained from different means.

	MD for Homogeneous cubic	MD for Nanoconfinement (at Bulk region)	Experiment [85]
$\rho\ (\sigma_{Ar}{}^{-3})$	0.800	0.800±0.01	0.8
$T\ (K)$	99.24	100.0±0.8	109.44
$P\ (atm)$	246.4	250.2±2.5 for (001) 260.5±2.0 for (111)	246.0

It is challenge to achieve an identical thermodynamic property for the various sizes of channels, especially a small channel that has no bulk region. This is because the inhomogeneous nature of fluid arrangement near interface due to the interplay between the solid and fluid atoms. As is well known, the interplay between wall and fluid molecules induce a dynamic fluid structure near the walls. This fluidic structure resembles the solid structure very adjacent to the wall. This structural similarity gradually diminishes and eventually exhibits general fluidic structure at distance of about 6~7 molecular distances

from the wall. Accordingly, the channel smaller than 12~14 molecular diameters do not exhibit bulk region making it difficult to determine the similar thermodynamic state. To deal with the problem, the first adsorbed layers were matched to have a certain value within an acceptable error. Prior to that, the bulk density of the large nanoconfinements (i.e. H_{ww} ≥6.946nm) were adjusted to 0.8 as shown in Table 2. These adjusting processes were done by trial and error to add and remove the atoms inside of the channel. The bulk region of the channels approximately is in the same thermodynamic state, $\rho_{bulk} \approx 0.8$, T ≈ 100K, $P_{bulk} \approx 250$ for (001), $P_{bulk} \approx 260$ for (001). It is noted that, our EMD simulation results shows that when the different sizes of channels are in a thermodynamic state, both the peak density and pressure are also almost identical. Based on this finding we adjust the peak density for the thin channels that have no bulk region to ensure an identical thermodynamic state. However, this method cannot perfectly ensure an identical thermodynamics state. When we check the peak pressure in Table 2, it starts to deviate at the channels that smaller than 2nm. In addition, the NPT ensemble cannot be an alternative for this problem. The NPT ensemble does not exactly consider the atomic-level wall/fluid interface. Although many studies have been performed using NPT ensembles, the use of NPT ensembles in nanochannels does not yield accurate results until the boundary problem will be solved.

Table 2. Equilibrium MD simulation results of confined argon in various sizes of channels and silver lattice orientations (001) and (111).

Silver Lattice orientation	H_{ww} (nm)	N_{Ar}	δ_{peak} (Å)	$\frac{2\delta_{peak}}{H_{ww}}$ (%)	ρ_{bulk} $(\sigma_{Ar}{}^{-3})$	ρ_{peak} $(\sigma_{Ar}{}^{-3})$	P_{bulk} (atm)	P_{peak} (atm)	T_{avg} (K)
(001) X = 36.78Å Y = 36.78Å A_c = 1352Å²	1.026	198	2.857	55.9		2.266		1824	100.05
	1.434	298	2.836	39.7		2.528		1560	99.53
	1.842	414	2.856	31.1		2.719		1465	99.75
	2.250	534	2.846	25.3		2.754		1601	99.78
	2.659	646	2.854	21.5		2.723		1652	100.06
	3.068	758	2.842	18.5		2.722		1667	100.06
	3.477	870	2.832	16.3		2.714		1624	99.66
	6.946	1822	2.850	8.2	0.8008	2.722	251.5	1600	99.46
	10.419	2774	2.838	5.4	0.8006	2.733	252.7	1614	99.75
	17.366	4677	2.834	3.3	0.7999	2.725	247.1	1624	99.73
	34.732	9436	2.838	1.6	0.8002	2.719	249.5	1629	99.70
(111) X = 35.03Å Y = 34.67Å A_c = 1214Å²	1.026	182	2.891	57.2		2.719		2599	100.13
	1.434	267	2.874	40.2		2.904		1967	100.17
	1.842	379	2.890	31.4		3.266		1962	99.21
	2.250	480	2.890	25.7		3.178		1930	99.44
	2.659	580	2.891	21.8		3.125		1961	99.64
	3.068	682	2.899	18.9		3.144		1985	100.20
	3.477	780	2.888	16.6		3.124		1977	99.95
	6.946	1636	2.893	8.3	0.8009	3.146	260.1	1950	99.62
	10.419	2491	2.889	5.5	0.7995	3.102	262.3	1916	99.66
	17.366	4201	2.892	3.3	0.8006	3.133	262.5	1951	99.90
	34.732	8475	2.893	1.7	0.8008	3.096	257.2	1913	99.57

4.4. Two-dimensional density distribution and surface corrugation

The inhomogeneous structure of fluid near the interface, which is also referred to as liquid layering, adsorption layers, or dynamic structuring of fluid is well-known phenomena that observed at the nanoscale. This distinctive phenomenon has been intensively studied in both experiments and computer simulation [27, 32, 34, 86-89]. However, the most of the studies were conducted via one-dimensional analysis, which ignores the molecular-level corrugation at solid/fluid interface. The corrugations may play an important role to understand the interfacial phenomena. Thus, we plotted two-dimensional density distribution in Figure 13. The atomic-level corrugation is clearly shown in Figure 13(a). It is noted that there are more concentrated fluid atoms adjacent to the solid atoms whereas few concentrations of fluids between solid atoms. This creates atomic level corrugations at the first fluidic adsorption layer as shown in Figure 13(a). And one notable thing is that this corrugation also exists at the second adsorption layer even though its variations were considerably lessened. This corrugation almost diminished at the third adsorbed fluid layer as can be seen in Figure 13(c). However, the layering along the direction perpendicular to the solid surface still exists after the third layer. Also, the atomic-level corrugation at the interface may be the evidence of the idea that the atomic-level solid/fluid boundary is not a plane but a wave-like surface. In the gap between the solid and fluid, electrons and fields exist, and these might be needed to be addressed to directly observe the atomic-level boundary. Thus, further studies on the boundary definition using a first-principle simulation that considers the electrons and its fields explicitly.

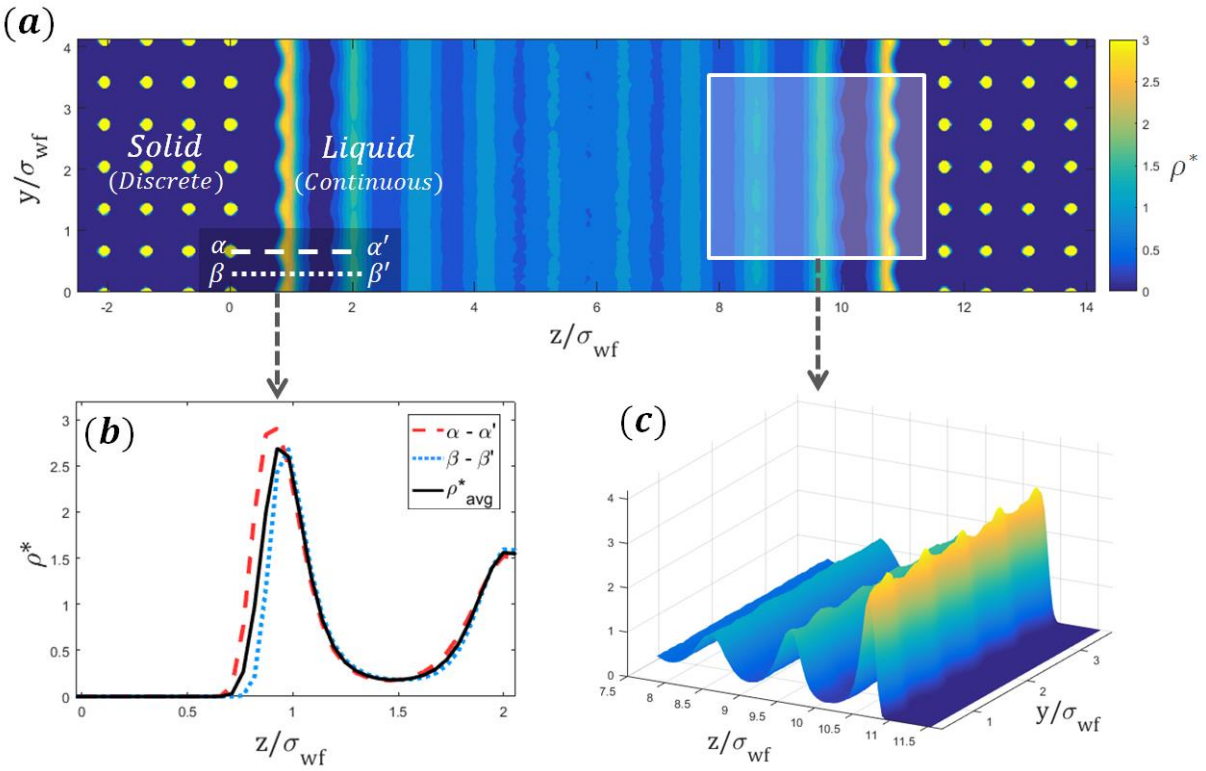

Figure 13. Density distributions in the silver argon nanoconfinement on (001) silver surface of (a) 2D view, (b) one-dimensional view at the peak and valley of atomic scale corrugation, (c) 2D contour of the atomic-level corrugation in the adsorbed fluid.

A zero density region was also found between the solid atoms and between solid and fluid in the 2D density plot (See Figure 13). This zero density region is the distinct difference between the continuum description of solid/liquid interface and molecular-based solid/liquid interface. Unfortunately, there is no theoretical tool to analyze the discrete system as its nature so far. Currently, we rely on the continuum based theories such as continuum mechanics and statistical mechanics. Thus, it is one of the challenges in the field of nano-engineering to develop an analytical model not based on the continuum description but the model that explicitly describes the atomistic system. The zero density

regions, which are also discussed in the previous section of local thermal equilibrium, depend on the thermal motion of fluid and solid atoms. However, the density calculation is shown in the present work, obtained by assuming that the all atomic mass concentrated on the center point of an atom. The zero density regions do not represent the totally empty region but it occupied by electrons and their potential field. It is noted that the distance between the first adsorbed layer and the innermost solid layer and the magnitude of the peak density is closely related with the interfacial thermal resistance [14, 47, 79, 83, 90, 91]. The studies reported that the large peak value results in a small interfacial thermal resistance and the short gap distance causes a small thermal boundary resistance. These tendencies explain that the origins of the thermal resistance at solid/fluid interface are an inefficient thermal transport between the discrete structure of solid and continuous structure of fluid as shown in Figure 13(a). This point of view on interfacial thermal resistance can explain why the surface orientation effects on the solid/fluid interfacial thermal resistance. In addition, several studies have shown that the one-dimensional gap distance is the general factor for the solid/fluid interfacial thermal resistance; however, the one-dimensional analysis of gap distance appears to be imperfect. In Figure 13(b), the gap distance varies depending on the cutting planes. Therefore, it is necessary to study gap distance which is two-dimensional or three-dimensional as in this study rather than gap distance defined in one-dimensional analysis.

4.5. Effects of boundary definition on determining average density in nanochannel

To demonstrate the effects of definition of solid/fluid boundary on thermodynamic property, we conducted equilibrium MD simulation at a thermodynamic state for various channels and two lattice orientations. First, we investigated the variations of average density according to the position where the boundary is defined. It is obvious that the average density can be estimated differently depending on the definition even in the identical system because the solid/fluid boundary definition is coupled with the fluid volume and the volume is related with the average density determination. To demonstrate the variation, the average density was examined by changing the definition of wall/fluid interface between $z_w = 0$ and $z_w = \sigma_{wf}$ via the following equation:

$$\rho_{Avg}(z_w) = \frac{1}{H_{ww} - 2z_w} \int_{z_w}^{H_{ww}-z_w} \rho^*(z)\, dz \tag{7}$$

Where H_{ww} is wall to wall height, z_w indicates the distance from the wall to the location of the interface, and the $\rho^*(z)$ represents the local number density. In Figure 4, the calculation of the average density varies depending on where the boundary is defined. As the boundary location, z_w, move from the innermost solid layer to the liquid region, the average density increase with decreasing volume in the zero density region. But, this increasing tendency is dwindling after the density depletion area and begins to decrease when the liquid molecular exclusion rate surpasses the rate of decreasing volume.

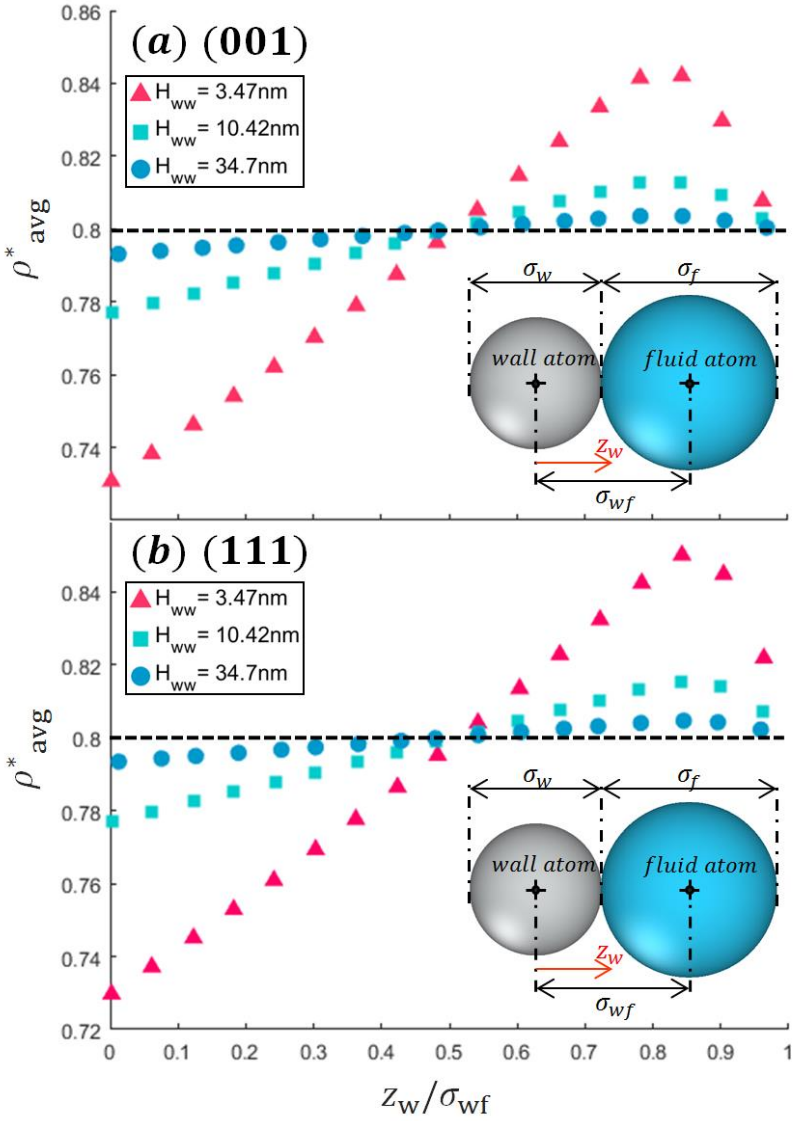

Figure 14. Average fluid density as a function of the location of the wall/fluid interface for the fcc (a) (001) and (b) (111) plane and three different sizes of the channel. The subfigure illustrates two LJ atoms and Lorentz-Berthelot mixing rule. The superscript, $*$, denotes the Lennard Jones dimensionless number. The dashed line describes ρ^*_{avg}=0.8.

Our results indicated that for the 3.47-nm channel, the average density varies from 0.73 to 0.84 depending on where the boundary is defined. Considering the fact that liquid is almost incompressible, this deviation can induce significant effects on interpreting the

thermodynamic state in nanochannels. It is important to note that, smaller channels are more sensitive to the definition of the interface because the small channel has the large ratio of the uncertainty. Interestingly, the average densities with the boundary definition of $z_w \cong 0.48\sigma_{wf}$ for the (001) crystal orientation and $z_w \cong 0.52\sigma_{wf}$ for the (111) crystal orientation are agree well with its bulk density (i.e $\rho_{bulk} = 0.8$) regardless of the channel sizes. According to this result, the average of the variation of density distribution is approximately the bulk density. Further research is needed to determine whether this phenomenon is confined to argon alone or to the thermodynamic state used in this study. Our results suggested that there was no noticeable difference in the result of the average density between the (001) and (111) planes. It is important to note that this problem can be avoided by using a local density distribution with fine bins. This effect of the boundary definitions is due to the ambiguity of the volume at the solid/fluid interface. Therefore, the fine bins that can display a full resolution of atomic concentration in the channel are barely affected by the definition of solid/fluid boundary. However, interpreting a channel using a density distribution instead of an average density is much more complicated than the conventional method and is poorly compatible with classical hydrodynamic theories. Thus, a novel theory that can explicitly analyze the inhomogeneous and discrete nature of nano-system is needed for a proper understanding of nano-channel transport phenomena.

4.6. Effects of boundary definition on estimating average pressure in nanochannel

After the average density investigation, we studied the effects of the boundary on pressure estimation. Similar with the density case, the average pressure estimation can be affected by the boundary definition. The microscopic description of pressure inherently contains the volume term as shown in the Eq (4). Hence, it is deduced that pressure calculation can be vary depending on where the wall/fluid boundary was defined. The average pressure exerted by the fluid was calculated by the following formula:

$$P_{Avg}(z_w) = \frac{1}{H_{ww} - 2z_w} \int_{z_w}^{H_{ww}-z_w} P(z)\ dz \tag{8}$$

Where H_{ww} represents wall to wall height, z_w is the distance from the wall to the location of the interface, and the $P(z)$ denotes the local number density. As shown in Fig. 5, the pressure calculation shows an increasing and decreasing tendency as the definition of the interface moves from the solid side to the liquid side. This is due to the inhomogeneous pressure distribution near solid surface due to the high variation of atomic concetration and the forces induced by solid atoms. The average pressure shows the scale effect that the small channel more sensitive to the definition of the wall/fluid interface. For a 3.47 nm channel, a calculation error of up to about 30 atmospheres can occur. This variation of pressure calculation may create disagreements among researchers. For example, the wall/fluid interface at the center of the innermost solid later, $z_w = 0$ is defined, the computed pressure decreases as the channel size decreases. On the other hand, for the wall/fluid interface at the $z_w = 0.5\sigma_{wf}$, the calculated pressures are almost constant regardless of the channel sizes. It clearly shows the how discrepancies in

conclusion can be created from the different definitions of boundary. Therefore, the absence of interfical definition is not only the problem of quantitive predictions but it also of understanding nanoscale phenomena.

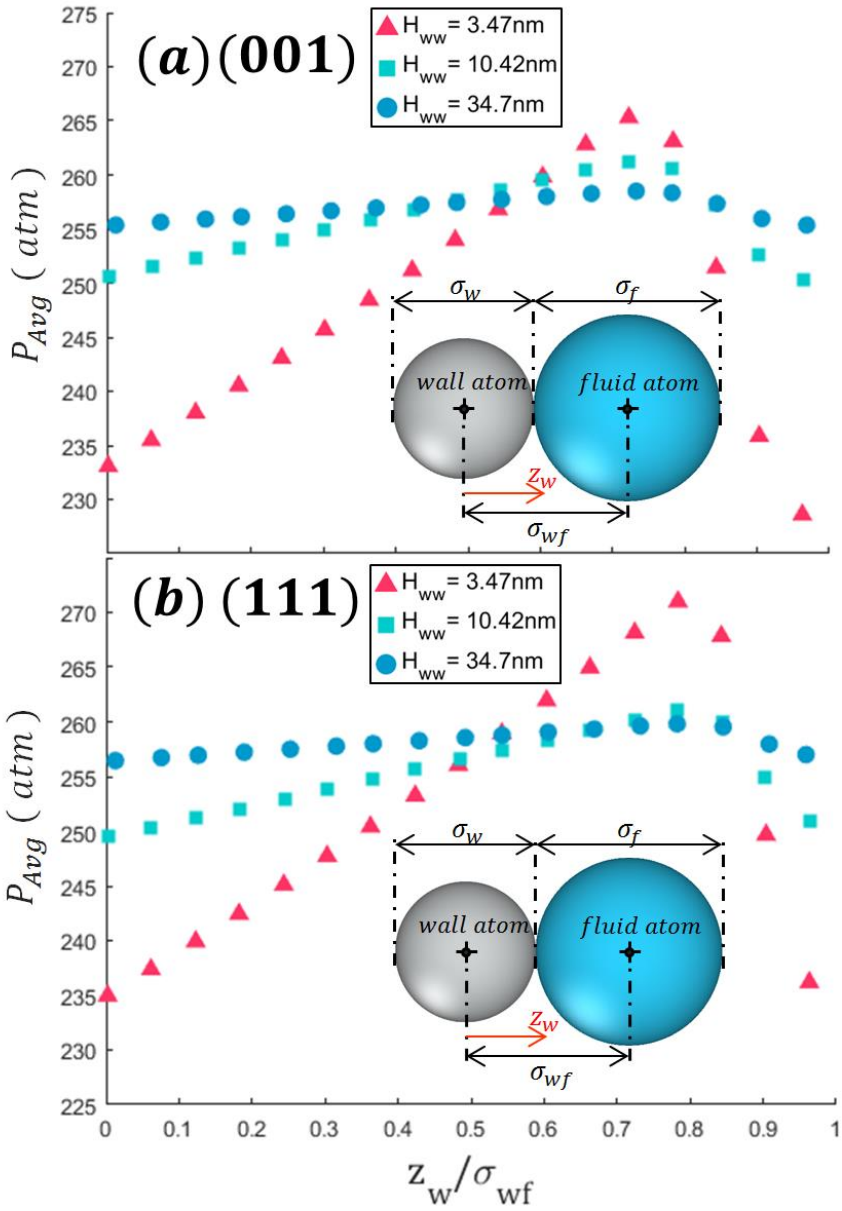

Figure 15. Average fluid pressure as a function of the location of the wall/fluid interface for the fcc (a) (001) and (b) (111) plane and three different sizes of the channel. The subfigure illustrates two LJ atoms and Lorentz-Berthelot mixing rule.

4.7. Atomic-level definition of solid/fluid boundary in heat transfer point of view

After the examination of the thermodynamic properties in the equilibrium system, heat transfer MD simulations were conducted in the confined environment. As mentioned in the methodology, the system has an averagely $0.01\ \mathrm{ev/ps}$ heat flux in steady state. The Irving-Kirkwood equation is commonly used to calculate the heat flux in an atomic simulation.

$$\mathrm{J} = \frac{1}{V}\sum_{k=1}^{N}\left[\sum_{i=1} e_i \mathrm{v}_i + \frac{1}{2}\sum_{i<j}(f_{ij}\cdot(\mathrm{v}_i + \mathrm{v}_j)\mathrm{x}_{ij})\right] \tag{9}$$

Where V is the volume of the system, N is the number of fluid atoms e_i is total energy of the atom i, f_{ij} is interatomic force acting on atom i by atom j, v_i and v_j are the velocity vecter of atom i and j respectively, and x_{ij} is the position vector between atom i and j. To calculate the heat flux across the fluid using Eq. 9, the fluid volume must be specified. Since we already know the heat flux of the system, we can determine the fluid volume satisfying the equation. From this fact, we have devised the following equation to elucidate the exact definition (location) of the liquid / solid interface by assuming that the definition of wall/fluid interface is plane and independent of temperatrue.

$$\mathrm{J}(z_w) = \frac{1}{A_c(H_{ww} - 2z_w)N}\sum_{k=1}^{N}\left[\sum_{i=1} e_i \mathrm{v}_i + \frac{1}{2}\sum_{i<j}(f_{ij}\cdot(\mathrm{v}_i + \mathrm{v}_j)\mathrm{x}_{ij})\right] \tag{10}$$

Where H_{ww} is wall to wall height, z_w represents the location of the interface, and A_c is the cross sectional area of the system. Generally, the heat flux calculation shows large fluctuations as discussed in the previous section, and thus the heat flux was computed during 20ns ~ 80ns, which is considerably longer than usual data collection time, 2ns.

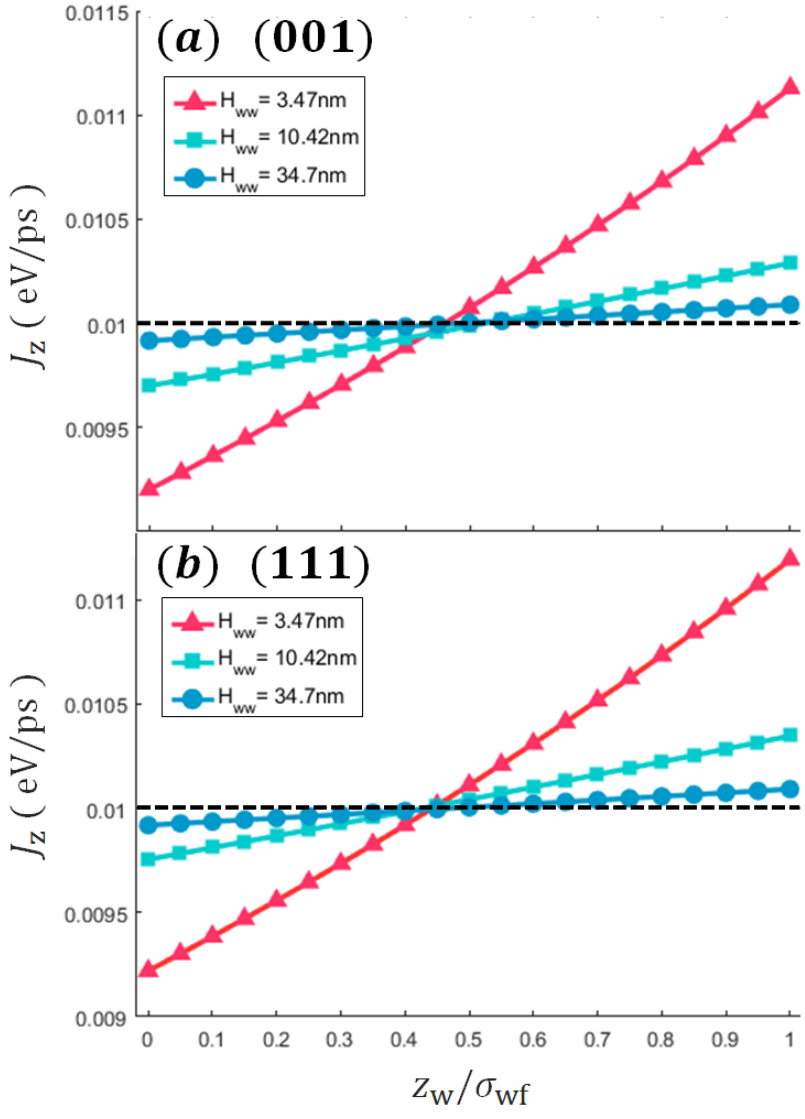

Figure 16. Estimations of the heat flux according to the definitions of the wall/fluid interface for three channels and (a) (001) and (b) (111) orientations. The given heat flux

was estimated by the system condition. The dashed line denotes the preset heat flux (i.e. 0.01 eV/ps)

Fig. 6 shows computed heat flux with respect to the defined location of wall/fluid interface proving improper definition of the wall/fluid interface causes errors in heat flux calculation. Heat flux computation are underestimated for the wall/fluid interface definition, *Innermost solid layer* (i.e. $z_w = 0$), whereas heat flux values are overestimated for the definition, *first density peak* (i.e. $z_w \approx \sigma_{wf}$). This deviation is greater in the smaller channel. Thus, it is expected that property assessment for an extremely thin channel like Carbon Nano Tube (CNT) will be highly dependent on the definition of the wall/fluid interface. The all lines cross at one point (i.e. $z_w \sim 0.45\sigma_{wf}$, $J = 0.01ev/ps$) regardless of channel sizes and crystal orientation. This location reasonably agrees with the location that recovers local viscosity in the study done by Kim *et al.* [41], '40% void volume of the first bins neighboring the walls' (i.e $z_w \sim 0.44\sigma_{wf}$). Also, interestingly, this position is well agrees with the location where the wall / fluid LJ potential represents zero (i.e. $z_w \sim 0.43\sigma_{wf}$) where is expected to be a solid/fluid interface at absolute zero temperature. Thus, we speculate that this region is approximate location of wall/fluid interface.

Thermal conductivity can be calculated theoretically by Green-Kubo method for equilibrium system [12, 78, 92], and Fourier's law for non-equilibrium systems [12, 24]. In case of Fourier's law, heat flux is necessary to estimate thermal conductivity. Consequently, when using the heat flux calculated by Eq. 6, the computed thermal conductivity displays the variations depending on the defined location of the wall/fluid

interface as shown in the Fig. 7. The thermal conductivity in the small channel shows high uncertainty making it difficult to pinpoint the thermal conductivity. The black dash line represents the thermal conductivity calculated by Green-Kubo Method with homogeneous LJ argon system, which contains 12,195 argon atoms with the approximately same thermodynamic state with the bulk region of nanoconfinement (See Table 1). It is noted that this system has no finite-size effects of thermal conductivity as it adopts the periodic boundary conditions to all directions. When comparing the homogeneous system with the nano-confinement system, thermal conductivity of confined liquid shows insignificant finite-size effects until 3.24nm channel, which can be explained by the short phonon mean free path of the liquid argon (one molecular diameter). The thermal conductivity from Green-Kubo method is within the variation of the thermal conductivity from Fourier's law near $0.4\sigma_{wf}$. This agreement of two thermal conductivity obtained by the systems with and without walls suggested that confined environment has no significant effects on liquid thermal conductivity, which idea is consistent with Xue *et al*. [32].

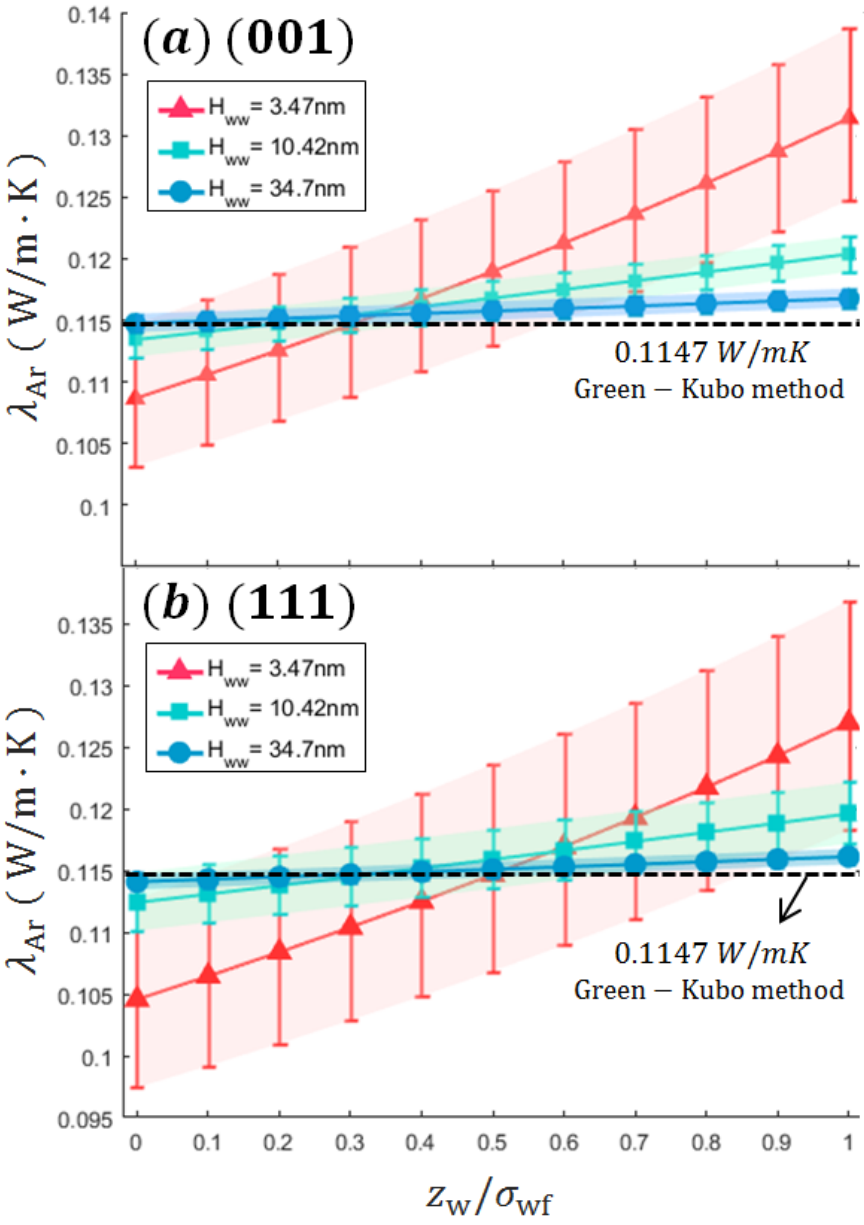

Figure 17. Estimated thermal conductivity based on the Fourier's law of conduction as a function of defined location of wall/fluid boundary for (a) (001) and (b) (111) orientations and three sizes of channels. The error bars were estimated as a standard deviation of linear regression of temperature gradient.

4.8. Scale effects of boundary definition

Our density, pressure, heat flux, and thermal conductivity investigations show scale effects due to the ambiguity of wall/fluid interface. Scale effect occurs because the ratio of the uncertainty is larger in small channel than large channel. The scale effect can be simply represented by the dimensionless parameter as the ratio of interfacial uncertainty to the channel size: $2\delta_{peak}/H_{ww}$ (Refer Table 2). In fluid mechanics, a dimensionless parameter is important to generalize the fluidic flow. For the nanochannel gas flow, Knudsen number is an important parameter to estimate how molecular-level behaviour dominant in the system. Likewise, the dimensionless parameter presented in the work, can roughly judge how the uncertainty of wall/fluid boundary acts significantly in the system according to channel size.

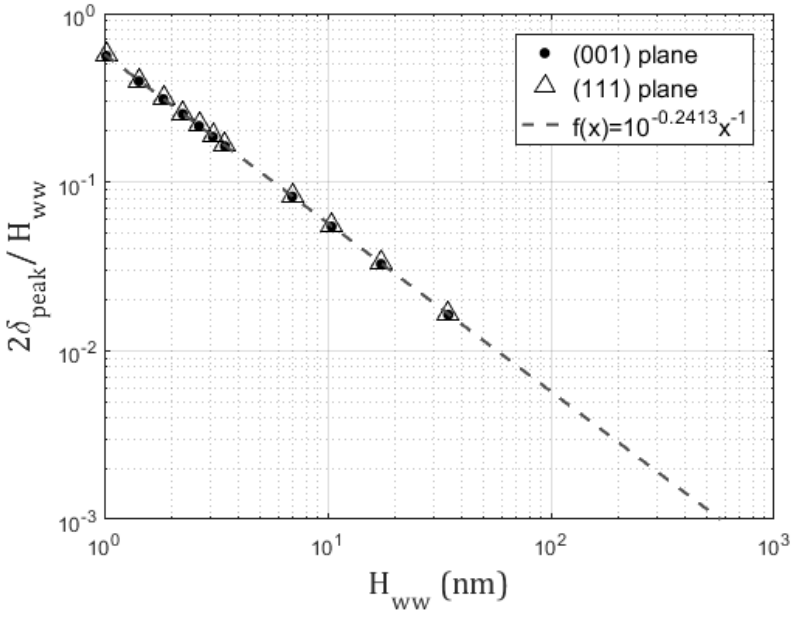

Figure 18. Quantification of the ambiguity rate of wall/fluid boundary. Both x and y axis represented as a log scale.

The ambiguity of wall/fluid interface is inversely proportional to the channel size as it is well linearized (See Figure 18). This quantification is analogous to but distinct from the dimensionless number suggested by Barisik et al. [59] in that the numerator is almost constant and the denominator is the channel size. They defined the ratio of wall force penetration depth (typically 3σ) to the channel widths and showed that wall force field plays a significant role in gas nano flows. This dimensionless parameter is useful to estimate the effects of boundary on the system scale.

4.9. Thermodynamic properties non-identical thermodynamic states.

After the investigation of nanochannel at a thermodynamic state, we investigate the effects of boundary definition on bulk density and peak density. In this additional study, five definitions of boundaries are considered from $z_w = 0$ to $z_w = \sigma_{wf}$ with $0.25\,\sigma_{wf}$ interval. As we already mentioned, ensuring a certain thermodynamic property for various sizes of channel is challenging and this step is important for comparing the results. Unlike to the previous studies, series of MD simulations were carried out with the average density fixed at 0.8 instead of setting the bulk and peak density. In these cases, the number of atoms inside of the channel varies with the definitions of solid/liquid boundary. These systematic discrepancies also have made in the nanoscale simulation field due to the absence of the rigorous definition of boundary. Therefore, this study can demonstrate what results are generated when researchers use different definitions of interface. Firstly, we investigate the density deviations according to the definition of boundary with channel sizes ranging from 1.02 nm to 34.7 nm.

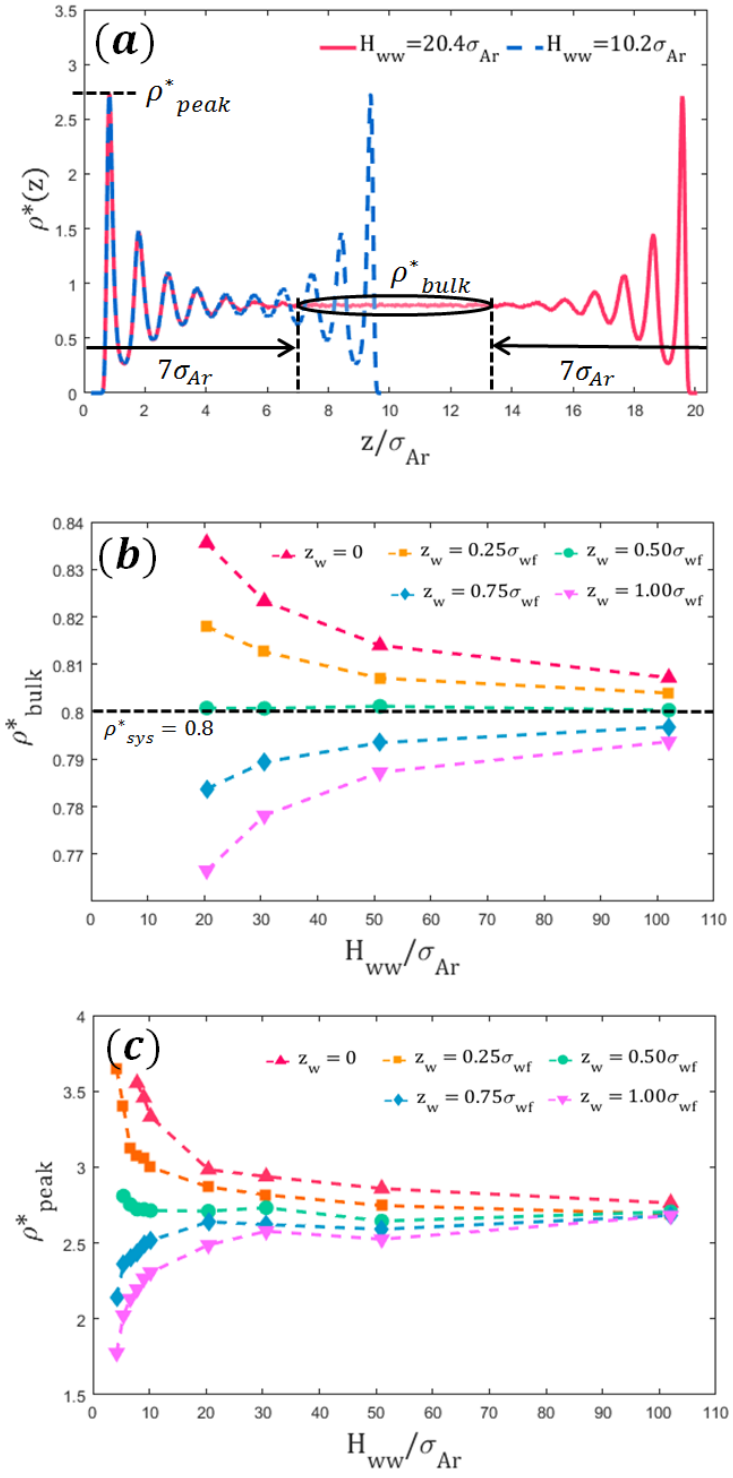

Figure 19. Density analysis in the various sizes of channels and various definitions of boundary: (a) full resolution of one dimensional density profiles, (b) bulk density with respect to the chanel size and (c) peak density with respect to the channel height

As shown in Figure 19(a), the bulk density was computed at the middle of the channels for the channel larger than 20 molecular diameters. The results of this demonstration show clearly how disagreements are created while analyzing the nanosystems. In Figure 19(b), on the basis of $0.5\,\sigma_{wf}$, the tendency of the bulk density with respect to the channel sizes are reversed. In other words, when we set the solid/fluid boundary at the innermost solid layer, then the numbers of atoms inside of the channel are overestimated while when we set the solid/fluid boundary at the first adsorbed layer, the numbers of atoms inside of the channel are underestimated. As the channel size increases, it converges to the asymptote value of 0.8. This result indicates that this effect is negligible at the large scale, which agrees well with the previous discussion. The peak density shows a similar tendency with the bulk density; however, the sensitiveness of the peak density on the boundary definition is greater due to the relatively smaller number of data for averaging than bulk density. None the less it clearly shows that the atomic-level boundary definition is imperative matter in the scale smaller than one digit nanometer. Thus, we must admit the importance of the boundary definition with atomic-level accuracy, and carefully deal with the nanoscale system as it is extremely sensitive to the boundary definition.

The local pressure near the interface exhibits high variations and it alleviates after several peaks in as shown in Figure 20 because of the surface forces and the interaction among solid and liquid molecules. We measured the bulk pressure in the mid-channel after 7 molecular diameters from the wall. A distinct peak and valley in a first adsorbed layer are observed. The bulk pressure is presented in Figure 20. Similar to the density study, the behavior of the bulk pressure is reversed on the basis of $z_w = 0.5\,\sigma_{wf}$. In addition, the

bulk pressure that was computed on the boundary definition, $z_w = 0.5\,\sigma_{wf}$, shows a good agreement with the bulk pressure estimated from the homogeneous MD simulation. This position would be not exactly the interface between liquid and solid, but it is inferred that there would be solid/fluid boundary in the vicinity of $z_w = 0.5\,\sigma_{wf}$.

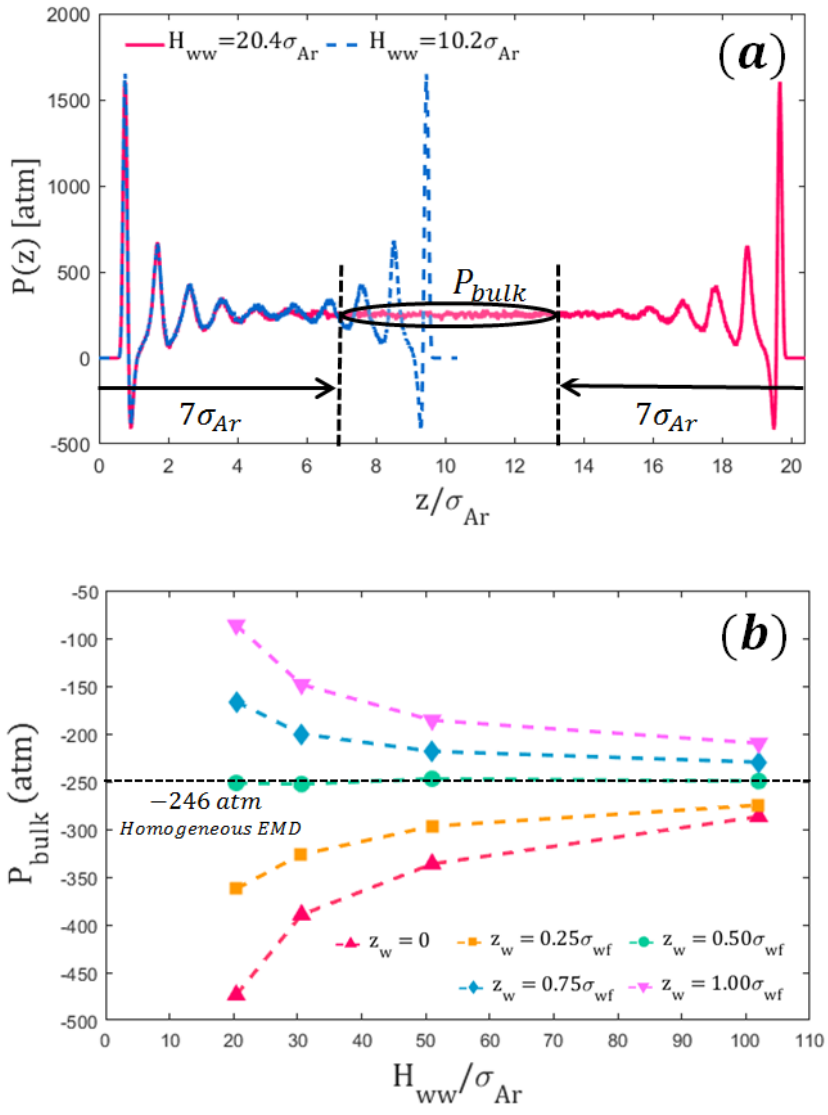

Figure 20. pressure analysis in the various sizes of channels and various definitions of boundary: (a) full resolution of one dimensional pressure profiles, (b) bulk pressure with respect to the chanel size and (c) peak pressure with respect to the channel height

5. Conclusion

In this work, we investigate the effects of the defined wall/fluid boundary on studying heat transfer in nanochannels using MD simulations. In the absence of an atomic-level boundary definition, the wall/fluid boundary has been defined between the innermost wall layer and the first adsorbed fluid layer creating one atomic diameter of the discrepancy. The challenges to defining wall/fluid boundary with atomic-level accuracy are related with the thermal motion of individual atoms, the discrete nature of small scale, the interatomic force penetration at interface, etc. We showed that the different definitions of boundaries could create severe impacts on understanding nanoscale physics as the surface-to-volume ratio becomes very large in nanosystems. To clarify the effects, non-equilibrium MD heat transfer simulations of liquid argon confined between two silver walls are conducted. Then, various channel heights were applied to observe the impact of the boundary definition with respect to the scale. Fluid density, heat flux across the channel, and the fluid thermal conductivity were calculated with respect to different wall/fluid boundary definitions. The results show that even though the approximate shift in the boundary was only one molecular diameter, the shift caused a relatively large deviation between the computed and the preset values. In addition, the deviation becomes more substantial with decreasing channel height. In case of 3nm channel, one atomic misplace of the boundary can significantly influence on average density and pressure inside of the channel. It is also revealed that depending on the boundary definition two contrast conclusions can be made on the tendency of thermal conductivity with respect to the

channel sizes. A precise definition of boundary is suggested where satisfying the microscopic heat flux expression. This definition is consistent with the previous report made by Kim *et al* [41] and also the zero-potential location of wall molecules, where is wall boundary in the absolute zero temperature. This result suggested that the temperature may have a little impact on the boundary location between wall and fluid. The findings in this work provide atomic-level insights into wall/fluid boundary, as well as valuable information on understanding nanoscale physics as well as the design of nanodevices.

REFERENCES

1. Anasori, B., Lukatskaya, M.R. & Gogotsi, Y. 2017, "2D metal carbides and nitrides (MXenes) for energy storage", *Nature Reviews Materials,* vol. 2, no. 2, pp. 16098.

2. Liu, K., Feng, J., Kis, A. & Radenovic, A. 2014, "Atomically thin molybdenum disulfide nanopores with high sensitivity for DNA translocation", *ACS nano,* vol. 8, no. 3, pp. 2504-2511.

3. Heiranian, M., Farimani, A.B. & Aluru, N.R. 2015, "Water desalination with a single-layer MoS 2 nanopore", *Nature communications,* vol. 6, pp. 8616.

4. Jiang, D., Cooper, V.R. & Dai, S. 2009, "Porous graphene as the ultimate membrane for gas separation", *Nano letters,* vol. 9, no. 12, pp. 4019-4024.

5. Brown, P.K., Qureshi, A.T., Moll, A.N., Hayes, D.J. & Monroe, W.T. 2013, "Silver nanoscale antisense drug delivery system for photoactivated gene silencing", *ACS nano,* vol. 7, no. 4, pp. 2948-2959.

6. Rojas, J.P., Singh, D., Inayat, S.B., Sevilla, G.A.T., Fahad, H.M. & Hussain, M.M. 2017, "Micro and Nano-Engineering Enabled New Generation of Thermoelectric Generator Devices and Applications", *ECS Journal of Solid State Science and Technology,* vol. 6, no. 3, pp. N3036-N3044.

7. Van Dessel, S. 2017, *Molecular thermoelectric lipid bilayers and a device using the same,* .

8. Feng, J., Graf, M., Liu, K., Ovchinnikov, D., Dumcenco, D., Heiranian, M., Nandigana, V., Aluru, N.R., Kis, A. & Radenovic, A. 2016, "Single-layer MoS 2 nanopores as nanopower generators", *Nature,* vol. 536, no. 7615, pp. 197.

9. Suzuki, I., Fukuda, M., Shirakawa, K., Jiko, H. & Gotoh, M. 2013, "Carbon nanotube multi-electrode array chips for noninvasive real-time measurement of dopamine, action

potentials, and postsynaptic potentials", *Biosensors and Bioelectronics,* vol. 49, pp. 270-275.

10. Park, M., Kang, B. & Jeong, K. 2018, "Based Biochip Assays and Recent Developments: A Review", *BioChip Journal,* vol. 12, no. 1, pp. 1-10.

11. Verlet, L. 1967, "Computer" experiments" on classical fluids. I. Thermodynamical properties of Lennard-Jones molecules", *Physical review,* vol. 159, no. 1, pp. 98.

12. Schelling, P.K., Phillpot, S.R. & Keblinski, P. 2002, "Comparison of atomic-level simulation methods for computing thermal conductivity", *Physical Review B,* vol. 65, no. 14, pp. 144306.

13. Ramos-Alvarado, B., Kumar, S. & Peterson, G. 2016, "On the wettability transparency of graphene-coated silicon surfaces", *The Journal of chemical physics,* vol. 144, no. 1, pp. 014701.

14. Ramos-Alvarado, B., Kumar, S. & Peterson, G. 2016, "Solid–Liquid Thermal Transport and Its Relationship with Wettability and the Interfacial Liquid Structure", *The journal of physical chemistry letters,* vol. 7, no. 17, pp. 3497-3501.

15. Ramos-Alvarado, B., Kumar, S. & Peterson, G. 2016, "Hydrodynamic slip length as a surface property", *Physical Review E,* vol. 93, no. 2, pp. 023101.

16. Hu, L., Desai, T. & Keblinski, P. 2011, "Determination of interfacial thermal resistance at the nanoscale", *Physical Review B,* vol. 83, no. 19, pp. 195423.

17. Hyżorek, K. & Tretiakov, K.V. 2016, "Thermal conductivity of liquid argon in nanochannels from molecular dynamics simulations", *The Journal of chemical physics,* vol. 144, no. 19, pp. 194507.

18. Park, S. & Sposito, G. 2002, "Structure of water adsorbed on a mica surface", *Physical Review Letters,* vol. 89, no. 8, pp. 085501.

19. Thomas, J.A., McGaughey, A.J. & Kuter-Arnebeck, O. 2010, "Pressure-driven water flow through carbon nanotubes: Insights from molecular dynamics simulation", *International journal of thermal sciences,* vol. 49, no. 2, pp. 281-289.

20. Sicard, E. 2017, "Introducing 7-nm FinFET technology in Microwind", .

21. Song, T., Jung, J., Rim, W., Kim, H., Kim, Y., Park, C., Do, J., Park, S., Cho, S. & Jung, H. 2018, "A 7nm FinFET SRAM using EUV lithography with dual write-driver-assist circuitry for low-voltage applications", *Solid-State Circuits Conference-(ISSCC), 2018 IEEE International*IEEE, , pp. 198.

22. Kim, M., Ha, D. & Kim, T. 2015, "Cracking-assisted photolithography for mixed-scale patterning and nanofluidic applications", *Nature communications,* vol. 6, pp. 6247.

23. Jung, W., Kim, J., Kim, S., Park, H.G., Jung, Y. & Han, C. 2017, "A Novel Fabrication of 3.6 nm High Graphene Nanochannels for Ultrafast Ion Transport", *Advanced Materials,* vol. 29, no. 17.

24. Kim, B.H., Beskok, A. & Cagin, T. 2008, "Molecular dynamics simulations of thermal resistance at the liquid-solid interface", *The Journal of chemical physics,* vol. 129, no. 17, pp. 174701.

25. Vo, T.Q. & Kim, B. 2018, "Physical origins of temperature continuity at an interface between a crystal and its melt", *The Journal of chemical physics,* vol. 148, no. 3, pp. 034703.

26. Kim, B. 2013, "Interface thermal resistance modeling of the silicon-argon interface", *International Journal of Precision Engineering and Manufacturing,* vol. 14, no. 6, pp. 1023-1028.

27. Nagayama, G. & Cheng, P. 2004, "Effects of interface wettability on microscale flow by molecular dynamics simulation", *International Journal of Heat and Mass Transfer,* vol. 47, no. 3, pp. 501-513.

28. Ramos-Alvarado, B., Kumar, S. & Peterson, G. 2016, "Hydrodynamic slip in silicon nanochannels", *Physical Review E,* vol. 93, no. 3, pp. 033117.

29. Barrat, J. & Bocquet, L. 1999, "Large slip effect at a nonwetting fluid-solid interface", *Physical Review Letters,* vol. 82, no. 23, pp. 4671.

30. Bhadauria, R., Sanghi, T. & Aluru, N. 2015, "Interfacial friction based quasi-continuum hydrodynamical model for nanofluidic transport of water", *The Journal of chemical physics,* vol. 143, no. 17, pp. 174702.

31. Bhadauria, R. & Aluru, N. 2013, "A quasi-continuum hydrodynamic model for slit shaped nanochannel flow", *The Journal of chemical physics,* vol. 139, no. 7, pp. 074109.

32. Xue, L., Keblinski, P., Phillpot, S., Choi, S. & Eastman, J. 2004, "Effect of liquid layering at the liquid–solid interface on thermal transport", *International Journal of Heat and Mass Transfer,* vol. 47, no. 19-20, pp. 4277-4284.

33. Włoch, J., Terzyk, A.P., Gauden, P.A., Wesołowski, R. & Kowalczyk, P. 2016, "Water nanodroplet on a graphene surface—a new old system", *Journal of Physics: Condensed Matter,* vol. 28, no. 49, pp. 495002.

34. Nguyen, C.T. & Kim, B. 2016, "Stress and surface tension analyses of water on graphene-coated copper surfaces", *International Journal of Precision Engineering and Manufacturing,* vol. 17, no. 4, pp. 503-510.

35. Raj, R., Maroo, S.C. & Wang, E.N. 2013, "Wettability of graphene", *Nano letters,* vol. 13, no. 4, pp. 1509-1515.

36. Vo, T.Q., Barisik, M. & Kim, B. 2015, "Near-surface viscosity effects on capillary rise of water in nanotubes", *Physical Review E,* vol. 92, no. 5, pp. 053009.

37. Huang, C., Nandakumar, K., Choi, P.Y. & Kostiuk, L.W. 2006, "Molecular dynamics simulation of a pressure-driven liquid transport process in a cylindrical nanopore using two self-adjusting plates", *The Journal of chemical physics,* vol. 124, no. 23, pp. 234701.

38. Hansen, J.S., Dyre, J.C., Daivis, P., Todd, B.D. & Bruus, H. 2015, "Continuum nanofluidics", *Langmuir*, vol. 31, no. 49, pp. 13275-13289.

39. Ghorbanian, J., Celebi, A.T. & Beskok, A. 2016, "A phenomenological continuum model for force-driven nano-channel liquid flows", *The Journal of chemical physics*, vol. 145, no. 18, pp. 184109.

40. Vo, T.Q. & Kim, B. 2016, "Transport phenomena of water in molecular fluidic channels", *Scientific reports*, vol. 6, pp. 33881.

41. Kim, B.H., Beskok, A. & Cagin, T. 2010, "Viscous heating in nanoscale shear driven liquid flows", *Microfluidics and nanofluidics*, vol. 9, no. 1, pp. 31-40.

42. Raghunathan, A., Park, J. & Aluru, N. 2007, "Interatomic potential-based semiclassical theory for Lennard-Jones fluids", *The Journal of chemical physics*, vol. 127, no. 17, pp. 174701.

43. Motevaselian, M. & Aluru, N. 2017, "An EQT-based cDFT approach for thermodynamic properties of confined fluid mixtures", *The Journal of chemical physics*, vol. 146, no. 15, pp. 154102.

44. Mashayak, S., Motevaselian, M. & Aluru, N. 2015, "An EQT-cDFT approach to determine thermodynamic properties of confined fluids", *The Journal of chemical physics*, vol. 142, no. 24, pp. 244116.

45. Han, H., Schlawitschek, C., Katyal, N., Stephan, P., Gambaryan-Roisman, T., Leroy, F. & Müller-Plathe, F. 2017, "Solid–Liquid Interface Thermal Resistance Affects the Evaporation Rate of Droplets from a Surface: A Study of Perfluorohexane on Chromium Using Molecular Dynamics and Continuum Theory", *Langmuir*, vol. 33, no. 21, pp. 5336-5343.

46. Barisik, M. & Beskok, A. 2014, "Temperature dependence of thermal resistance at the water/silicon interface", *International Journal of Thermal Sciences*, vol. 77, pp. 47-54.

47. Pham, A.T., Barisik, M. & Kim, B. 2014, "Molecular dynamics simulations of Kapitza length for argon-silicon and water-silicon interfaces", *International journal of precision engineering and manufacturing,* vol. 15, no. 2, pp. 323-329.

48. Vo, T.Q. & Kim, B. 2015, "Interface thermal resistance between liquid water and various metallic surfaces", *International Journal of Precision Engineering and Manufacturing,* vol. 16, no. 7, pp. 1341-1346.

49. Ramos-Alvarado, B., Kumar, S. & Peterson, G. 2016, "Solid–Liquid Thermal Transport and Its Relationship with Wettability and the Interfacial Liquid Structure", *The journal of physical chemistry letters,* vol. 7, no. 17, pp. 3497-3501.

50. Han, H., Mérabia, S. & Müller-Plathe, F. 2017, "Thermal Transport at Solid–Liquid Interfaces: High Pressure Facilitates Heat Flow through Nonlocal Liquid Structuring", *The journal of physical chemistry letters,* vol. 8, no. 9, pp. 1946-1951.

51. Shin, H., Yang, S., Chang, S., Yu, S. & Cho, M. 2013, "Multiscale homogenization modeling for thermal transport properties of polymer nanocomposites with Kapitza thermal resistance", *Polymer,* vol. 54, no. 5, pp. 1543-1554.

52. Pham, A., Barisik, M. & Kim, B. 2013, "Pressure dependence of Kapitza resistance at gold/water and silicon/water interfaces", *The Journal of chemical physics,* vol. 139, no. 24, pp. 244702.

53. Nagayama, G., Matsumoto, T., Fukushima, K. & Tsuruta, T. 2017, "Scale effect of slip boundary condition at solid–liquid interface", *Scientific Reports,* vol. 7, pp. 43125.

54. Koplik, J., Banavar, J.R. & Willemsen, J.F. 1989, "Molecular dynamics of fluid flow at solid surfaces", *Physics of Fluids A: Fluid Dynamics,* vol. 1, no. 5, pp. 781-794.

55. Geysermans, P., Gorse, D. & Pontikis, V. 2000, "Molecular dynamics study of the solid–liquid interface", *The Journal of chemical physics,* vol. 113, no. 15, pp. 6382-6389.

56. Chen, G. 2005, *Nanoscale energy transport and conversion: a parallel treatment of electrons, molecules, phonons, and photons,* Oxford University Press.

57. Heyes, D.M. 1994, "Pressure tensor of partial-charge and point-dipole lattices with bulk and surface geometries", *Physical Review B*, vol. 49, no. 2, pp. 755.

58. Long, Y., Palmer, J.C., Coasne, B., Śliwinska-Bartkowiak, M., Jackson, G., Müller, E.A. & Gubbins, K.E. 2013, "On the molecular origin of high-pressure effects in nanoconfinement: The role of surface chemistry and roughness", *The Journal of chemical physics*, vol. 139, no. 14, pp. 144701.

59. Thompson, A.P., Plimpton, S.J. & Mattson, W. 2009, "General formulation of pressure and stress tensor for arbitrary many-body interaction potentials under periodic boundary conditions", *The Journal of chemical physics*, vol. 131, no. 15, pp. 154107.

60. Shi, Z., Barisik, M. & Beskok, A. 2012, "Molecular dynamics modeling of thermal resistance at argon-graphite and argon-silver interfaces", *International Journal of Thermal Sciences*, vol. 59, pp. 29-37.

61. Amani, A., Karimian, S. & Seyednia, M. 2017, "A molecular dynamics simulation on the effect of different parameters on thermal resistance of graphene-argon interface", *Molecular Simulation*, vol. 43, no. 4, pp. 276-283.

62. Vogelsang, R., Hoheisel, C. & Ciccotti, G. 1987, "Thermal conductivity of the Lennard-Jones liquid by molecular dynamics calculations", *The Journal of chemical physics*, vol. 86, no. 11, pp. 6371-6375.

63. Liang, Z. & Tsai, H. 2011, "Effect of molecular film thickness on thermal conduction across solid-film interfaces", *Physical Review E*, vol. 83, no. 6, pp. 061603.

64. Ghorbanian, J. & Beskok, A. 2016, "Scale effects in nano-channel liquid flows", *Microfluidics and Nanofluidics*, vol. 20, no. 8, pp. 121.

65. Liu, C., Cohen, J., Adams, J. & Voter, A. 1991, "EAM study of surface self-diffusion of single adatoms of fcc metals Ni, Cu, Al, Ag, Au, Pd, and Pt", *Surface Science*, vol. 253, no. 1-3, pp. 334-344.

66. Williams, P., Mishin, Y. & Hamilton, J. 2006, "An embedded-atom potential for the Cu–Ag system", *Modelling and Simulation in Materials Science and Engineering,* vol. 14, no. 5, pp. 817.

67. Wu, H.H. & Trinkle, D.R. 2009, "Cu/Ag EAM potential optimized for heteroepitaxial diffusion from ab initio data", *Computational Materials Science,* vol. 47, no. 2, pp. 577-583.

68. Liang, Z. & Keblinski, P. 2015, "Slip length crossover on a graphene surface", *The Journal of chemical physics,* vol. 142, no. 13, pp. 134701.

69. Niu, D. & Tang, G. 2016, "The effect of surface wettability on water vapor condensation in nanoscale", *Scientific reports,* vol. 6, pp. 19192.

70. Frolov, T. & Mishin, Y. 2010, "Orientation dependence of the solid–liquid interface stress: atomistic calculations for copper", *Modelling and Simulation in Materials Science and Engineering,* vol. 18, no. 7, pp. 074003.

71. Balasubramanian, G., Banerjee, S. & Puri, I.K. 2008, "Unsteady nanoscale thermal transport across a solid-fluid interface", *Journal of Applied Physics,* vol. 104, no. 6, pp. 064306.

72. Puliti, G., Paolucci, S. & Sen, M. 2011, "Thermodynamic properties of gold–water nanolayer mixtures using molecular dynamics", *Journal of Nanoparticle Research,* vol. 13, no. 9, pp. 4277-4293.

73. Plimpton, S. 1995, "Fast parallel algorithms for short-range molecular dynamics", *Journal of computational physics,* vol. 117, no. 1, pp. 1-19.

74. Stukowski, A. 2009, "Visualization and analysis of atomistic simulation data with OVITO–the Open Visualization Tool", *Modelling and Simulation in Materials Science and Engineering,* vol. 18, no. 1, pp. 015012.

75. Lin, S., Blanco, M. & Goddard III, W.A. 2003, "The two-phase model for calculating thermodynamic properties of liquids from molecular dynamics: Validation for the phase

diagram of Lennard-Jones fluids", *The Journal of chemical physics,* vol. 119, no. 22, pp. 11792-11805.

76. Kubo, R. 1957, "Statistical-mechanical theory of irreversible processes. I. General theory and simple applications to magnetic and conduction problems", *Journal of the Physical Society of Japan,* vol. 12, no. 6, pp. 570-586.

77. Green, M.S. 1954, "Markoff random processes and the statistical mechanics of time-dependent phenomena. II. Irreversible processes in fluids", *The Journal of chemical physics,* vol. 22, no. 3, pp. 398-413.

78. Volz, S.G. & Chen, G. 2000, "Molecular-dynamics simulation of thermal conductivity of silicon crystals", *Physical Review B,* vol. 61, no. 4, pp. 2651.

79. Alexeev, D., Chen, J., Walther, J.H., Giapis, K.P., Angelikopoulos, P. & Koumoutsakos, P. 2015, "Kapitza resistance between few-layer graphene and water: Liquid layering effects", *Nano letters,* vol. 15, no. 9, pp. 5744-5749.

80. Hu, M. & Poulikakos, D. 2013, "Graphene mediated thermal resistance reduction at strongly coupled interfaces", *International Journal of Heat and Mass Transfer,* vol. 62, pp. 205-213.

81. Hu, M., Goicochea, J.V., Michel, B. & Poulikakos, D. 2009, "Water nanoconfinement induced thermal enhancement at hydrophilic quartz interfaces", *Nano letters,* vol. 10, no. 1, pp. 279-285.

82. Vo, T.Q., Barisik, M. & Kim, B. 2016, "Atomic density effects on temperature characteristics and thermal transport at grain boundaries through a proper bin size selection", *The Journal of chemical physics,* vol. 144, no. 19, pp. 194707.

83. Torii, D., Ohara, T. & Ishida, K. 2010, "Molecular-scale mechanism of thermal resistance at the solid-liquid interfaces: influence of interaction parameters between solid and liquid molecules", *Journal of Heat Transfer,* vol. 132, no. 1, pp. 012402.

84. Bin Saleman, A.R., Chilukoti, H.K., Kikugawa, G., Shibahara, M. & Ohara, T. 2017, "A molecular dynamics study on the thermal transport properties and the structure of the solid–liquid interfaces between face centered cubic (FCC) crystal planes of gold in contact with linear alkane liquids", *International Journal of Heat and Mass Transfer,* vol. 105, pp. 168-179.

85. Tegeler, C., Span, R. & Wagner, W. 1999, "A new equation of state for argon covering the fluid region for temperatures from the melting line to 700 K at pressures up to 1000 MPa", *Journal of Physical and Chemical Reference Data,* vol. 28, no. 3, pp. 779-850.

86. Vo, T.Q., Park, B., Park, C. & Kim, B. 2015, "Nano-scale liquid film sheared between strong wetting surfaces: effects of interface region on the flow", *Journal of Mechanical Science and Technology,* vol. 29, no. 4, pp. 1681-1688.

87. Asproulis, N. & Drikakis, D. 2011, "Wall-mass effects on hydrodynamic boundary slip", *Physical Review E,* vol. 84, no. 3, pp. 031504.

88. Sun, Y., Zhang, F., Ye, Z., Ding, Z., Mendelev, M.I., Kramer, M.J., Wang, C. & Ho, K. 2017, "Structural ordering at solid-liquid interfaces in Al-Sm system: A molecular-dynamics study", *Materials Letters,* vol. 186, pp. 26-29.

89. Gao, J., Luedtke, W. & Landman, U. 1997, "Layering transitions and dynamics of confined liquid films", *Physical Review Letters,* vol. 79, no. 4, pp. 705.

90. Asproulis, N. & Drikakis, D. 2010, "Boundary slip dependency on surface stiffness", *Physical Review E,* vol. 81, no. 6, pp. 061503.

91. bin Saleman, A.R., Chilukoti, H.K., Kikugawa, G., Shibahara, M. & Ohara, T. 2017, "A molecular dynamics study on the thermal energy transfer and momentum transfer at the solid-liquid interfaces between gold and sheared liquid alkanes", *International Journal of Thermal Sciences,* vol. 120, pp. 273-288.

92. Che, J., Çağın, T., Deng, W. & Goddard III, W.A. 2000, "Thermal conductivity of diamond and related materials from molecular dynamics simulations", *The Journal of chemical physics,* vol. 113, no. 16, pp. 6888-6900.

Curriculum Vitae
(2018 June)

Yechan Aaron Noh (노예찬)

Micro/Nano-scale Thermo-Fluids Engineering Laboratory (MNTF) by 2018 June
University of Ulsan 93 Daehak-ro, Nam-gu,
Ulsan (44610), South Korea

E-mail: olrzro@mail.ulsan.ac.kr
Site: https://sites.google.com/site/yechannoh/
Lab Site: http://home2.ulsan.ac.kr/user/nanofluid/

RESEARCH INTERESTS

Fundamental/Theory

- Multi-scale Modeling
  (First principles - Nanoscale dynamics)
  (Nanoscale - Continuum)
- Interfacial Phenomena

Applications

- Nanopores
- Energy Storage Device
- Lab on a Chip
- Thermal Management

EDUCATION

University of Ulsan, Republic of Korea March 2011 - August 2016
B. E. in Mechanical Engineering
Research Advisor: Dr. BoHung Kim
Overall GPA: 3.94/4.00 (***Rank 01/258*** and Junior-Senior GPA 4.00/4.00)

University of Ulsan, Republic of Korea August 2016 –August 2018
M. E. in Mechanical Engineering
Academic Advisor: Professor. BoHung Kim
Specialized in Nanoscale Interfacial Phenomena and Molecular Dynamics Simulation and Numerical Analysis
Overall GPA: 4.00/4.00

RESEARCH EXPERIENCE

University of Ulsan, Republic of Korea Jun 2016 – June 2018
Graduate Research Assistant

- **Effects of Boundary Definitions of Molecular Scale Solid/Liquid Interface**: a close investigation of solid/liquid interface was conducted by using molecular dynamic simulation to elucidate the exact location of the interface. This study showed that the atomic-level boundary definition is essential for proper understanding of nanoscale physics. A dimensionless parameter to estimate the scale effects is suggested. Also atomic-level definition on heat transfer point of view is proposed.
- Modeling of the heat exchanger of Free Piston Stirling Engine that utilizes exhausted heat from diesel engine as heat source using finite volume method: the purpose of this work is to amplify the heat transfer but minimize pressure drop before and after the heat exchanger.
- Mixing Analysis of Agitator for Desulfurization System: the object of this project is to design the rotational speed and ideal position and orientation of the impeller to ensure a certain mixing ratio. Multiphase flow, Multi-Reference Frame, and Periodic Boundary Condition were utilized in this work.

University of Ulsan, Republic of Korea August 2014 – Jun 2016
Undergraduate Research Assistant

- Computational Fluid Dynamics (CFD) Modeling of Multi Cyclone: the goal of this project is to reduce pressure drop while maintaining the dust collection efficiency. A parametric study was conducted for each cyclone to build a database of pressure drops. With this database, the evaluation method of total pressure drop for the multi-cyclone was suggested.
- Multiscale flow Analysis of Working Fluid in Stirling Engine using Molecular Dynamics Simulation and Computational Fluid Dynamics: thermodynamics and material properties in harsh condition were extracted through the molecular dynamics simulation. With these properties, the dynamic, transient CFD analysis was conducted employing dynamic mesh technique.

SCHOLARSHIPS, AWARDS, AND HONORS

- ***National Science and Engineering Undergraduate Scholarship*** granted by Korean Government and Korea Student Aid Foundation 2015 – 2016
- ***Summa Cum Laude Honor*** granted by University of Ulsan to the student with highest GPA in Mechanical Engineering Program at the University of Ulsan. August 2016
- Best Academic Achievement Award granted by the University of Ulsan 2014, 2015, 2016

TEACHING EXPERIENCE

University of Ulsan, Republic of Korea
Teaching Assistant

- Mechanical Engineering Experiment G03324. An experimental course in mechanical engineering for the undergraduate students. Gave students an introduction to the methodology of the experiment at 2016 fall and 2017 fall.
- Creative Engineering Design G03226. A basic Designing course in mechanical engineering for undergraduate students using Lab view based software and computer built-in assembly block at 2017 spring.

SKILLS

- Molecular Dynamics Simulation: LAMMPS
- Visualization: OVITO, VMD
- Computing Tool: MATLAB
- CFD Analysis: FLUENT
- Program Language: C++

ACTIVITIES

- Republic Of Korea Marine Corps, ROKMC May 2012 - February 2014
- Life Guard at the Mangsang Beach in Korea July 2014 - August 2014
- Student Union Member, Sub-Director of Physical Activity, in Mechanical Department 2011
- Member of the football team, ‘Machine,' 2011 - present